

Development and characterization of tissue engineered 3D scaffolds based on gelatin methacryloyl microbeads

A thesis presented for the
M.Sc. in Nanotechnologies for ICTs

Department of Electronics and Telecommunications
POLITECNICO DI TORINO
Academic year 2017/2018

Supervisors

Prof. Danilo Demarchi
Prof. Maurizio Martina

Candidate

Outman Akouissi

Host supervisors

Prof. Ali Khademhosseini
Amir Sheikhi, PhD.



Developed at the Khademhosseini laboratory,
University of California, Los Angeles

*A mamma e papà,
per i vostri grandi sacrifici.
A Beppe, Milena e Marica,
per avermi messo sulla strada migliore.*

Development and characterization of tissue engineered 3D scaffolds based on gelatin methacryloyl microbeads

Developed at the Khademhosseini Laboratory at UCLA, USA

Supervisors

Prof. Danilo Demarchi
Prof. Maurizio Martina

Candidate

Outman Akouissi

Host supervisors

Prof. Ali Khademhosseini
Amir Sheikhi, PhD.

Abstract

One of the focus areas in tissue engineering is biofabrication, that is the in-vitro creation of functional and biomimetic models of tissues and organs with applications ranging from wound healing to in vitro personalized drug development. One of the main challenges in this field is the manufacturing of 3D cell culturing scaffolds, to develop bioinspired functional tissue models in vitro. A wide range of biomaterials has been developed, with gelatin methacryloyl (GelMA) being one of the most promising: it is in fact a hydrogel featuring low cost, high cell adhesion affinity and high versatility. This work presents a novel GelMA-based scaffold fabrication technique, using annealed microfluidically-generated microbeads. An innovative protocol exploiting the temperature-responsiveness of the polymer is described for the first time. Both individual beads and annealed structures are thoroughly characterized, showing novel properties such as independent porosity from stiffness, an essential feature needed for bone tissue engineering. Finally, cell culturing studies performed on the beaded scaffolds show promising results for future applications of this innovative platform.

Acknowledgments

My deepest gratitude goes to Prof. Demarchi, without whom developing this thesis wouldn't have been possible and whose mentoring for the last three years has made me a better engineer. I am grateful to Prof. Ali Khademhosseini for hosting me in his laboratory. I sincerely thank Amir Sheikhi, PhD, for the interesting brainstorming sessions and for putting me in charge of the GelMA microbeads project: his trust and motivation allowed me to work harder and better than ever before. Huge thanks to Reihaneh Haghniaz, PhD, and Joe De Rutte, for their immense patience in teaching me from my first day in this project and for their constant support throughout my whole stay at UCLA. Thanks to Alireza Sohrabi for the help in performing the AFM measurements.

I am grateful to all lab members for the great times in and out of the lab.

My experience at UCLA wouldn't have been the same without the support of my friend, flatmate and classmate Alessandro, whom I thank for accompanying me in this intense adventure.

Getting to this moment wouldn't have been possible without the support of my enlarged family: my parents and Marica, Milena and Beppe Ferrero. My gratitude also goes to the outstanding people I met on my way: my friends at the San Liborio dorm, who've been like a second family to me while in Turin. Special thanks to Enrica, for being there to lift me up whenever I needed despite the distance and Tanya, whose jokes and laughs made any situation easier to face. Thanks to Fedele, for the great adventures and hard work together for the last five years and through four countries. Thanks to Massimo, for the support when needed and for the continuous stimulus to try harder and aim higher. Thanks to all my great Nanotech classmates, for the mutual support and the fun times throughout the last two years.

Thanks to Sarah, for the stimulating discussions, the support given and for making every day special.

Contents

1	Introduction, Motivations and Goals	17
1.1	Tissue engineering	17
1.1.1	3D cell cultures	18
1.1.2	Biomaterials	19
1.2	Droplet microfluidics	20
1.2.1	Principles	21
1.2.2	Applications in tissue engineering	22
1.3	Beaded 3D scaffolds	22
1.3.1	State of the art	22
1.3.2	Goals	23
2	Materials and Methods	25
2.1	Materials	25
2.1.1	Microfluidics	25
2.1.2	GelMA synthesis	26
2.1.3	Microbead processing	26
2.1.4	Cell culturing	26
2.1.5	Characterization instruments	27
2.2	Methods	27
2.2.1	Fabrication of the microfluidic device	28
2.2.2	Gelatin methacryloyl synthesis	28
2.2.3	Bulk GelMA scaffolds fabrication	28
2.2.4	GelMA bead fabrication	29
2.2.5	GelMA beads handling protocol	29
2.2.6	Pore size measurement	30
2.2.7	Mechanical analysis	30
2.2.8	Rheology studies	31
2.2.9	Temperature stability studies	31
2.2.10	Swelling and shrinking analysis	32
2.2.11	Atomic Force Microscopy indentation studies	32
2.2.12	Cell culture	33
2.2.13	3D cell encapsulation	33
2.2.14	Metabolic activity assessment	34
2.2.15	3D cell migration	34
2.2.16	Live/Dead assay	34

3	Results and discussion	35
3.1	GelMA bead fabrication	35
3.2	Microbead processing and scaffold fabrication	36
3.3	Temperature stability studies	37
3.4	Swelling and shrinking studies	38
3.5	Pore size characterization	39
3.6	Mechanical characterization	41
3.6.1	Compression	42
3.6.2	Tensile	42
3.6.3	AFM	43
3.6.4	Rheology	44
3.7	Cell studies	45
3.7.1	Cell encapsulation	46
3.7.2	Cell penetration	48
4	Conclusions and Perspectives	51
4.1	Conclusions	51
4.2	Perspectives	52

List of Figures

1.1	(A) Schematic indicating the cycle for organ replacement in tissue engineering, extracted and adapted from [20] (B) Schematic illustrating a sample Body-on-a-Chip system, extracted from [23]	18
1.2	(A) Illustration of a spheroid with a necrotic core, highlighting other layers and gradients throughout its structure, adapted from [37].(B) Example of multi layer vascularized scaffold, fabricated using soft lithography, adapted from [17].(C) Example of 3D printed vascularized structure achieved through a sacrificial lattice, adapted from [29].	19
1.3	(A) Schematic of a T-junction microfluidic droplet generator (B) Schematic of a flow-focus microfluidic droplet generator, adapted from [4].	21
1.4	Sample applications of hydrogel droplets in tissue engineering. (A) Cell adhesion (i) and encapsulation (ii) schematics, (B) Schematic of spheroid-based 3D printing steps, (C) Example of injectable (i), annealable (ii) and cytocompatible(iii) bead-based wound healing technology, adapted from [3, 31, 12].	22
2.1	Standard (A) and positive displacement (B) pipettes compared: when dispensing special liquids, such as high viscosity gels, standard pipettes dispense less than the full volume. Positive displacement pipettes instead deliver the full volume thanks to the tight piston pushing the liquid all the way through.	27
2.2	Schematic drawing illustrating the crosslinking setup. Pressing the top slide allows the creation of highly uniform samples for repeatable measurements.	29
2.3	Mechanical characterization setups using the Instron testing column: (A) Compression, (B) Tensile.	31
2.4	Pictures illustrating the algorithm used to automatically measure the equivalent diameters of the beads when imaged using brightfield microscopy: (A) Original image in grayscale, (B) Thresholded image, (C) Bead filling and Watershed algorithm application, (D) Identified bead edges.	32
2.5	Pictures illustrating the AFM tip morphology and operation when used in tapping mode to evaluate the Young compression modulus of a single GelMA microbead.	33
2.6	Schematic of the cell experiments to be performed on the scaffolds.	34

3.1	(A) Plot showing the versatility of the flow-focus droplet generation device, generating beads with diameter from circa 70 μm to 120 μm by altering the flow ratio, (B) Picture of the device in operation, scale bar indicates 500 μm , (C) GelMA microbeads in oil, scale bar indicates 100 μm	36
3.2	Beaded scaffold pictures showing: (A) Brightfield microscopy image, (B) Self-standing structure and shape, (C) Ease of handling. Scale bar indicates 250 μm	37
3.3	Table summarizing the results of the temperature stability studies. The pictures are a sample of those used for deriving the data plotted on the side. Scale bars indicate 200 μm	38
3.4	Shrinking and swelling behaviors of non-crosslinked GelMA microbeads immersed in hypertonic or hypotonic solutions, scale bars indicate 200 μm	39
3.5	Shrinking and swelling behaviors of individually crosslinked GelMA microbeads immersed in hypertonic or hypotonic solutions, scale bars indicate 200 μm	39
3.6	Top and orthographic views of the 3D reconstruction of the porous architecture of the beaded GelMA scaffolds. The voids represent the spaces occupied by microbeads while pores are represented by the green-dyed structures. The sample consists of 20 % GelMA beads annealed for 120 s.	40
3.7	(A) Extract from the pore analysis script showing how each slice is processed, interconnected pore areas are tagged and their areas evaluated to finally calculate void fraction and median pore size, (B) Void fraction at different scaffold annealing times, (C) Median pore size for the same scaffolds. Scale bars indicate 250 μm	41
3.8	(A) Curves displaying the compressive stress vs strain behavior of beaded and bulk GelMA scaffolds crosslinked for 60, 120 and 180 s. (B) Logarithmic plot of the compression moduli derived from the stress vs strain curves.	42
3.9	(A) Curves displaying the tensile stress vs strain behavior of beaded and bulk GelMA samples annealed, and therefore crosslinked, for 60, 120, 180 s. (B) Tensile moduli derived from the stress vs strain curves.	43
3.10	(A) Curves displaying the tensile stress vs strain behavior of GelMA microbeads and bulk samples, crosslinked for 60, 120, 180 s. (B) Compressive moduli derived from the stress vs strain curves. It can be appreciated how both GelMA morphologies share comparable stiffness values.	44
3.11	Rheological properties of beaded GelMA scaffolds compared to their bulk counterparts in terms of storage (A) and loss (B) moduli versus angular frequency. Range of measurements between 0.1 rad s^{-1} and 100 rad s^{-1}	44
3.12	(A) Storage moduli at frequency $\sim 1 \text{ rad s}^{-1}$ and $\sim 0.1 \%$ strain, evaluated for bulk and beaded GelMA scaffolds. (B) Same as the adjacent image but relative to the loss moduli. 0 crosslinking time in beaded samples indicates non annealed structures.	45

3.13	(A) Fluorescence microscope images of 3T3 cells embedded inside the beaded GelMA scaffolds after live/dead staining, with timepoints up to day 7 (B) Day 1 live/dead staining of the same cells embedded into bulk GelMA scaffolds. Scale bars indicate 500 μm	46
3.14	Fluorescence and brightfield images overlay, showing a close-up of the beaded GelMA structure, where cell adhering to the beads surface are spreading through the pores. 3T3 cells stained with live/dead staining. Scale bar indicates 100 μm	47
3.15	(A) Plot indicating the ratio between live and dead cells in the images displayed in figure 3.13 (B) PrestoBlue TM assay fluorescence intensity readings, performed up to 14 days after incubation.	47
3.16	(A) Lateral view of the 3D reconstruction representing the cell penetration of the HUVEC cells into a bulk GelMA substrate, after 1 hour (B) Orthographic view of the same. Sides are 1550 μm long and height is 254 μm high	48
3.17	(A) Lateral view of the 3D reconstruction representing the cell penetration of the HUVEC cells into a beaded GelMA substrate, after 1 hour (B) Orthographic view of the same. Sides are 1550 μm long and height is 254 μm high	49

Chapter 1

Introduction, Motivations and Goals

1.1 Tissue engineering

Tissue engineering is a technical field emerged in the last 30 years, synergizing the knowledge from disciplines apparently far from each other: medicine, engineering and science [5]. The main goal of the discipline is the manufacturing of artificial biological tissues or synthetic substitutes that are biomimetically functional, controllable and reproducible. Tissue engineering aims to face multiple challenges: in an ever aging population, organ failure and therefore organ replacements are some of the major burdens for the healthcare systems worldwide [11]. As of 2015, less than 10 % of the patients in need of a transplant have a corresponding donor, making it necessary to recur to expensive chronic therapies and surgeries for the rest of the patients in need. Tissue engineering proposes an alternative solution, aiming to cancel the need of an organ donor, replacing it with human tissues or organs grown and engineered in vitro, starting from samples and cells from the patient itself.

Another challenge targeted by tissue engineers is the development of drugs and therapies for one of the deadliest diseases of the 21st century, cancer, killing up to 8.2 millions people just in 2012 [10]. Cancer is the result of the anomalous cell behavior growing in unregulated manner, invading multiple parts of the body to finally kill the host. Because of its own patient-specific nature, being each cancer different from person to person, it is challenging to diagnose and cure the disease in a targeted manner: doctors often recur to highly invasive therapies that sacrifice some healthy tissues to get rid of the malign bodies, chemotherapy is an example. In this case tissue engineering may provide a game-changing tool: the possibility of reproducing a patient's cancer in vitro, creating fully functional and highly accurate models called Cancer-on-a-Chip [38], would provide a powerful platform for testing newly developed drugs or combinations of them to finally formulate personalized therapies, hopefully in time to cure the disease. A further step in this direction would be the development of more complex models, with the goal of mimicking the patient's complete body, integrating different organs and tissue models and therefore creating what is called Human-on-a-Chip: such platform would constitute the ultimate tool for drug testing, providing a useful test-bench for novel drugs and therapies and reducing the impact of side effects on healthy tissues [28]. Moreover, the compact nature of these Organ-on-a-Chip devices and their evolutions simplifies the handling

and study of the cell and the tissue constructs their form: built on common materials such as silicones and glass, it is easy to perform microscopy studies, integrate biosensors for biomarker detection and control vital parameters such as temperature and oxygen levels, creating completely automatic systems controllable with tailored software and electronics [39].

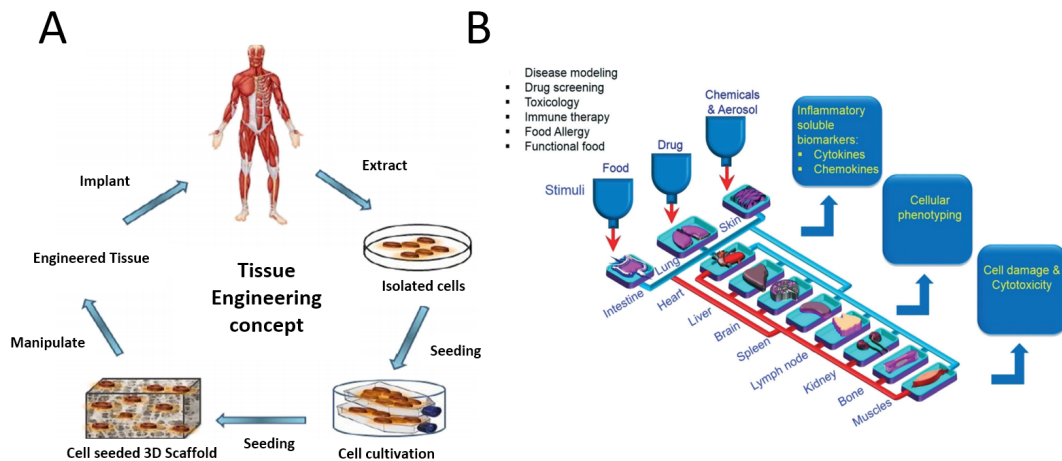


Figure 1.1: (A) Schematic indicating the cycle for organ replacement in tissue engineering, extracted and adapted from [20] (B) Schematic illustrating a sample Body-on-a-Chip system, extracted from [23]

1.1.1 3D cell cultures

Until 1980 biologists used hard substrates, such as glass or plastic dishes, to culture and grow bacteria and cells. This approach allowed them to develop single or double layers of cells and perform studies on drugs, vaccines, cell metabolism and more. However, complex biological systems such as humans are three-dimensional in nature, where the spatial orientation and localization of cells determines their role in the tissue. Moreover, tissues have different physical properties such as stiffness, transparency and so on, that are intrinsically influencing the cell behavior and vice-versa [34]. Knowing this, 3D cell culture techniques have emerged, with the goal of mimicking the natural environments. To develop effective Organ-on-a-Chip devices it is therefore necessary to resort to 3D models of the tissues of interest.

The earliest examples of 3D cultures are achieved using spinning flasks, where the cell suspensions are constantly stirred, allowing the cells to adhere only with each other and not to the flask's surface, prompting the formation of aggregates called spheroids. With this system it is also possible to achieve co-cultures of different cell types, forming what are called organoids, allowing inter-cell signaling and physical interaction, thus creating more realistic models. However organoids and spheroids have a main limiting factor for their growth: cell necrosis at the core. This is caused by diffusion [9], the transport mechanism delivering oxygen and nutrients to the cells and similarly carrying waste away from them. Once the spheroid diameter increases over a limit size, cells in the core fail to receive enough nutrients and to dispose of their debris, inevitably dying [37]. This is an issue common to other 3D cell culture techniques, such as those based on solid scaffolds like electrospun fibers and other

porous substrates [24], or those based on simple gel supports, such as hydrogels, in which small molecule diffusion is one of the many challenges [30].

This obstacle to growth is not present in living beings thanks to vascularization, that can deliver nutrients to all cells through a dense capillary network. To further mimic nature, bioinspired designs are developed, artificially creating microchannels and porous structures that allow the flow and better penetration of the culture media and molecules of interest [17]. Some examples on the rise nowadays are soft lithography-based multilayer structures and 3D printed vascularized scaffolds.

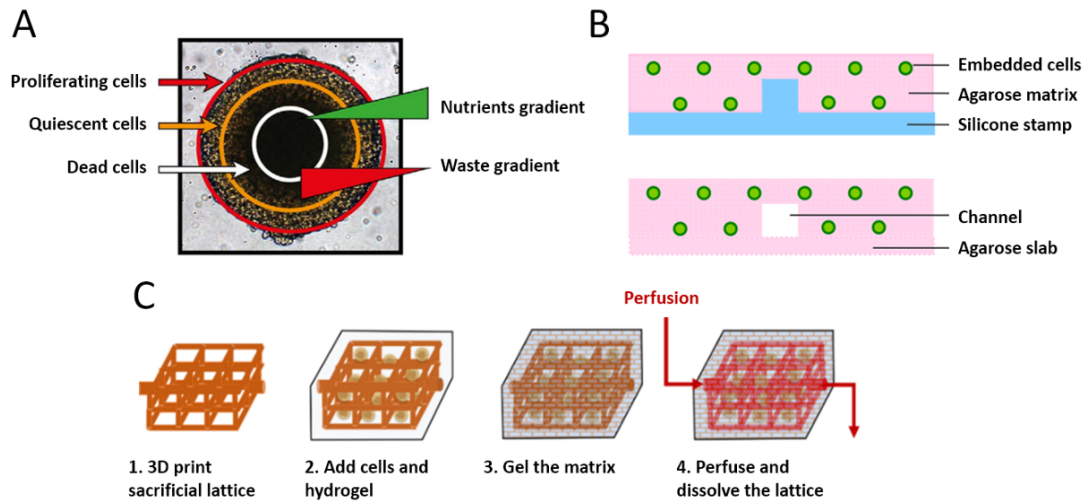


Figure 1.2: (A) Illustration of a spheroid with a necrotic core, highlighting other layers and gradients throughout its structure, adapted from [37].(B) Example of multi layer vascularized scaffold, fabricated using soft lithography, adapted from [17].(C) Example of 3D printed vascularized structure achieved through a sacrificial lattice, adapted from [29].

1.1.2 Biomaterials

To build effective biomimetic 3D tissues it is necessary to understand the complexity of the different environments in which cells are growing. For example, it is obvious that the bone tissue is stiffer than the muscular one and has different electrical properties than brain tissue. In fact, cells are embedded into what is called Extracellular Matrix (ECM), a collection of molecules secreted by cells with the goal of supporting, both physically and biochemically, the cellular network forming the tissue. Collagen is one of the most common molecules present in all ECMs, however bone ECM is characterized also by the presence of minerals that confer stiffness: the main one is hydroxyapatite, constituting up to 70% in bone weight [19]. Similarly, each tissue type is characterized by its own chemical composition and therefore physical properties.

Also the spatial orientation of the cells forming a tissue is critical for the correct functionality of the same: the most common example is the muscular tissue, where myocytes are aligned to contract the whole muscle in an efficient manner. Moreover, ECMs present also gradients in composition characterized by complex geometries: for example, this can be seen in every junction between different tissues such as the bone-tendon-muscle interface.

Decellularized organs are scaffolds used for 3D cultures, these present the highest fidelity to their natural counterparts to date. However, since based on the availability of explanted organs, it does not provide scalability, one of the key features required in tissue engineering. For this reason, a plethora of biomaterials has been developed to mimic the ECM, each with different characteristics depending on the intended applications: among these, hydrogels stand out for their promising properties such as ease of processing, high hydrophilicity, tunability, cell compatibility and similarity to the natural extracellular matrix [6]. Hydrogels can be inorganic or organic, the latter are usually preferred for 3D cell culture applications since they allow the construction of scaffolds with chemical and biological properties closer to the originals in nature. One of the most interesting properties of hydrogels is the possibility to trigger controlled gelation, therefore tuning the viscosity or even stiffness in the case of solidified structures [25]. Hydrogels can be designed with a wide range of molecules, such as chitosan and poly(ethylene glycol) to cite some, and properties such as conductivity, transparency, porosity, stiffness, printability and more. However, this work is focused on a promising polymer: gelatin methacryloyl.

Gelatin methacryloyl

Gelatin methacryloyl (GelMA) is a hydrogel derived from gelatin, to which a majority of methacrylamide groups and a minority of methacrylate ones are conjugated. GelMA has desirable properties for scaffold biofabrication: for example, the high amount of arginine-glycine-aspartic acid (RGD) sequences present, that is naturally occurring in gelatin, promotes cell adhesion and proliferation. Another key property is the possibility of crosslinking, with the addition of photoinitiators, either via irradiation (using UV or visible light) or via chemical reaction: this allows the creation of controlled structures with tunable porosity and stiffness [36]. Thanks to its numerous properties and mixing with other compounds and molecules, GelMA has found a large number of applications in tissue engineering: from wound healing biomaterials [40] to 3D scaffold for cell cultures, the full potential of this material is yet to be discovered. Joining forces with microfluidics for example, another set of applications can be derived: stiffness of molecular gradients can be created, allowing the creation of more realistic tissue interface models [21].

Another interesting application of GelMA is the design and creation of artificially vascularized tissues in vitro: controlling different parameters such as viscosity via temperature (GelMA is thermally sensitive) or polymer concentration, it is possible to 3D print complex structures, electrospin highly porous scaffolds and use lithography techniques to fabricate intricate micron-sized channels in a bulk substrate.

1.2 Droplet microfluidics

Droplet microfluidics generate finite volumes of liquid phase as a dispersion into another non-miscible phase, creating droplets with volumes down to the femtoliter. The applications of such technology span from the food industry to pharmaceuticals and also tissue engineering.

1.2.1 Principles

The basic principle allowing the formation of droplets is the presence of two or more immiscible phases, usually an oil and a water-based solution, allowing the formation of spherical droplets: to avoid the merging between each other, a naturally occurring phenomenon aiming to reduce the interfacial energy between phases, surfactants are added to one of the phases. Generally, droplet microfluidics aim to the creation of uniform-volume droplets: this can be achieved exploiting soft lithography techniques, fabricating very accurate devices for highly uniform droplet size distributions. In few words, all devices share the presence of at least two flows: the continuous flow, that is the suspension's medium, and the dispersed flow, that is the one forming droplets. A wide variety of geometries are developed, each with specific applications and properties: the simplest example is constituted by the so-called "T junction" where a microchannel carrying one of the two phases meets another channel in which the opposite phase is flowing, at the crossing point droplets are then formed by pinching at the corner. Another example of geometry for droplet microfluidics is called "Flow focus" and consists of two pinching channels carrying the same phase, these are incident perpendicularly from both sides on a third channel carrying the other phase. This geometry allows a more precise control of droplet size, achieving smaller volumes with respect to a T junction with same channel sizes [13]. These are two of the many possible designs that can be used for the generation of droplets, additional layers of complexity can be added to achieve features such as mixing, core-shell structures, cell or particle encapsulation and so on. Moreover, given the high precision in manufacturing and the presence of laminar flow proper of microfluidics, it is possible to accurately and empirically characterize the operation of such devices [2] depending on channel sizes, flow rates, viscosities, densities and surface tension. For example, an empirical law is available to predict the behavior of droplets in a "T junction": $\frac{L}{a} \approx 1 + \frac{Q_d}{Q_c}$ where L is the length of the plug, a the width of the oil channel, Q_d and Q_c are the discontinuous and continuous phase flow rates respectively. The two geometries introduced previously are displayed in figure 1.3.

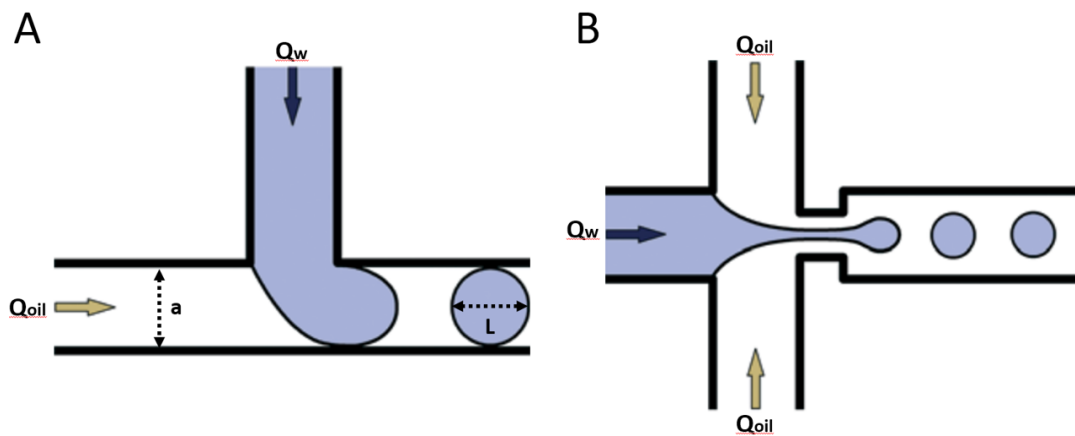


Figure 1.3: (A) Schematic of a T-junction microfluidic droplet generator (B) Schematic of a flow-focus microfluidic droplet generator, adapted from [4].

1.2.2 Applications in tissue engineering

Droplet microfluidic devices can be used to create microparticles for drug delivery in cellularized scaffolds or to process liquid-phase biomaterials, such as hydrogels, opening up new possible applications and scaffold geometries for tissue engineering. Some sample applications of this technology consist in the fabrication of hydrogel microbeads acting as support for the surface adhesion, and later penetration, of cells [15]. Researchers have extensively studied technologies for the encapsulation of cells in hydrogel droplets, using a broad combination of polymers, oils and cell types. These constructs can be used, as an example, for the development of wound healing technologies, providing support and protection to the cells injected [3]. Another application is the creation of organoids suspended in culture media, that can be later used for high throughput drug studies [1] or 3D printing, where uniform organoid size distribution is key to achieve high spatial resolution [31]. Finally, more complex but promising applications involve the usage of hydrogel microbeads to develop novel 3D scaffold geometries, with properties that overcome some of the limitations of other 3D cell culture and Organ-on-a-Chip technologies.

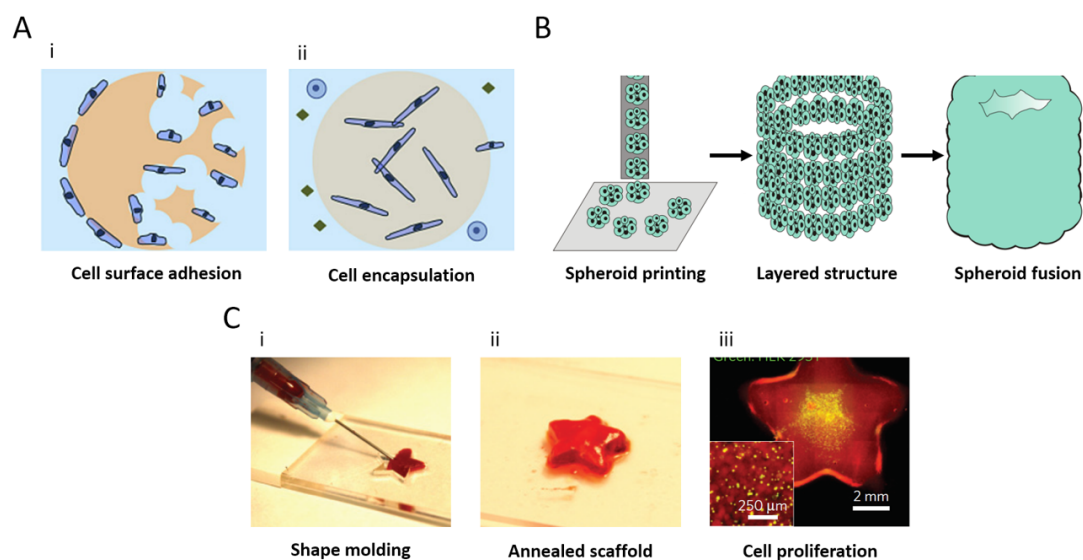


Figure 1.4: Sample applications of hydrogel droplets in tissue engineering. (A) Cell adhesion (i) and encapsulation (ii) schematics, (B) Schematic of spheroid-based 3D printing steps, (C) Example of injectable (i), annealable (ii) and cytocompatible(iii) bead-based wound healing technology, adapted from [3, 31, 12].

1.3 Beaded 3D scaffolds

As introduced in the previous section, hydrogel microbeads generated via droplet microfluidics have great potential for applications in tissue engineering. This work focuses on beaded scaffolds, using gelatin methacryloyl (GelMA) as biomaterial.

1.3.1 State of the art

While no examples of GelMA-based beaded scaffold are available in current literature, results obtained using other biomaterials can be found: an example is the work

carried by the group led by Professor Shoji Takeuchi at the University of Tokyo. One of their most interesting papers deals with the development of macroscopic 3D tissues using collagen microbeads, coated with cells and molded together [18]. As an interesting addition, microbeads are also used to when encapsulating liver cells and coated with fibroblasts: this combination allows the formation of millimeter-sized tissues that are self standing thanks to the adhesion between cells, that secrete the essential ECM molecules. Another research group used hyaluronic acid beads to fabricate scaffolds in which fibroblast are seeded and growing, spreading around the microspheres [27]. Others did use the beaded structures as a mold, generating scaffold with the same geometry as the pore network in between the beads [35].

1.3.2 Goals

The goal of this work is to develop a new architecture for the fabrication of 3D cell culture scaffolds using GelMA: until now this biomaterial has been 3D printed, patterned and electrospun (as indicated in section 1.1.2). Therefore, since no data are available, a microbead manipulation protocol must be elaborated and a thorough characterization carried. With the support of the well validated knowledge on the bulk GelMA characteristics, new properties can be predicted, such as the independence between porosity and stiffness.

With the help of microfluidic droplet generation devices, GelMA bead production is characterized, at different polymer concentrations. Then a robust handling protocol is invented, requiring less chemical processing than the other techniques: this is possible thanks to the possibility to physically (and temporarily) crosslink GelMA via temperature modulation, allowing the cleaning from the oil and the resuspension in a water-based buffer solution. Choosing one of the multiple well consolidated crosslinking techniques, in this case using a photoinitiator activated by UV radiation, beads are crosslinked individually or annealed to each other forming self-standing scaffolds. Individual beads are characterized mechanically to be compared to their bulk counterparts. Moreover the same and additional studies are performed on the scaffolds: rheology, porosity and cell culturing experiments are also carried and analyzed in this thesis. A specific polymer concentration, 20 % w/v GelMA in Phosphate Buffer Solution (PBS), is used to show one of the many possible advantages of this platform: in fact, such a high concentration does not allow cell encapsulation in bulk scaffolds, as the very high stiffness and low porosity induce cell death. Therefore, using this technology to fabricate stiff and porous scaffolds, it is possible to develop 3D bone tissue models.

This work is intended as the starting point of a hopefully fertile set of projects in which the properties of GelMA beaded scaffold are exploited to the fullest.

Chapter 2

Materials and Methods

In this chapter, a detailed description of the materials used and the methods followed are provided.

2.1 Materials

The materials used in this work can be categorized in five main areas of application: microfluidics for bead fabrication, GelMA synthesis, microbead processing, cell culturing and finally characterization tools used for this study.

Almost all applications involve the use of deionized water (DI water), obtained from a Milli-Q water filtration system provided by Millipore Corporation (MA, USA), with an electrical resistivity of $\sim 18.2 \text{ M}\Omega \text{ cm}$ at 25°C .

2.1.1 Microfluidics

The flow-focus microfluidic device was fabricated using standard soft lithography materials, in our case silicon wafers (University Wafer, MA, USA) were used as substrate, negative photoresist (KMPR 1050, MicroChem Corp., MA, USA) was patterned, and polydimethylsiloxane (PDMS) base and the curing agent (SYLGARDTM 184 Elastomer Kit, Dow Corning, MI, USA) were used to fabricate the device in se. Standard microscope glass slides were used as substrate for the patterned PDMS. A fluorophilic surface coating, Aquapel[®] Glass Treatment (Pittsburgh Glass Works LLC (PA, USA)) was applied to the internals of the microfluidic device in order to assure proper flow for the oil phase. The liquids were actuated using standard plastic syringes of different volumes mounted on configurable syringe pumps (Harvard Apparatus PHD 2000, MA, USA). Tygon plastic flexible tubing (0.02" ID x 0.06" OD (Saint-Gobain PPL Corp., CA, USA)) was used to connect the different parts of the system, while 1569-PEEK Tubing Orange 1/32" OD x .020" ID (IDEX Corp., IL, USA) was used to plug into the PDMS device to reduce flow resistance and simplify the insertion.. The oil phase consists of a fluorinated oil, NovecTM 7500 Engineered Fluid 3M (MN, USA). This oil was selected because of its viscosity, similar to water, its hydrophobic and lipophobic properties and its oxygen permeability, essential when encapsulating cells into droplets. To enable micro-droplet formation and avoid merging, a surfactant is needed: in this case, Pico-SurfTM 1 (5% (w/w) in NovecTM 7500) (Sphere Fluidics Inc (Cambridge, UK)) was chosen as it is specifically engineered for droplet microfluidics using NovecTM 7500, it is non-cytotoxic

and easily washable.

2.1.2 GelMA synthesis

The gelatin methacryloyl was synthesized starting from Type-A gelatin from porcine skin (300 bloom), supplemented with methacrylic anhydride (MA, 94%). The photoinitiator (PI) used for this work was 2-hydroxy-1-(4-(hydroxyethoxy)phenyl)-2-methyl-1-propanone (also known with the commercial name, Irgacure 2959), all manufactured by Sigma-Aldrich (MO, USA). The latter was chosen given its low cytotoxicity for a large range of cell types and its high crosslinking efficiency [33]. Osmotic filtering was performed with a dialysis membrane with 12-14 kDa molecular weight cutoff (MWCO), provided by Spectrum Lab Inc (CA, USA), WhatmanTM 1440-090 filter paper was distributed by GE Healthcare (IL, USA). Lyophilization was performed using a Labconco FreeZone 4.5L freeze-dryer (Labconco, MO, USA). Dulbecco's Phosphate Buffer Saline (DPBS) was purchased from Gibco (NY, USA). The GelMA solution was filtered using the low protein binding Acrodisc Syringe Filters with Supor Membrane, Sterile - 0.2 μm , 25 mm (Pall Corp., NY, USA). Other materials used include standard hotplates, glassware and microcentrifuge microtubes of various volumes from Eppendorf (Germany).

2.1.3 Microbead processing

The materials used to handle the microbeads and prepare the different samples include: 1H,1H,2H,2H-Perfluoro-1-octanol (PFO) 97% to break the GelMA-oil emulsion and fluorescein isothiocyanate-dextran solution (500 kDa) for pore visualization, both purchased from Sigma-Aldrich. Microscope cover slips (No.1.5) by VWR (PA, USA), were used as substrate for confocal imaging. The beads in suspension were packed using a GmCLab mini centrifuge (Gilson, France), spinning at a speed of 6300 rpm. To properly transfer beads between different containers, a Positive Displacement pipette, MICROMAN[®] E by Gilson (WI, USA), was used. This was necessary given the viscosity of the microbead suspension, that makes regular air-piston pipettes ineffective in the dispensing step, as shown in figure 2.1. Samples were fixed to glass slides for the AFM measurements using Cell-Tak as adhesive (Corning, NY, USA) and fixed to a paper holder using Crazy Glue (Elmer's Products, NC, USA) for the tensile measurements. Samples were crosslinked using an Omnicure Series 2000 UV source (360 nm to 480 nm) (Excelitas, CA, USA), linked to a UV blocking box through a 5 nm optical fiber.

2.1.4 Cell culturing

NIH/3T3 fibroblast cells and human umbilical vein endothelial cells (HUVECs) were purchased from the American Type Culture Collection (ATCC, VA, USA). Fetal bovine serum (FBS), penicillin/streptomycin (P/S), Dulbecco's modified Eagle medium (DMEM), DPBS solution (1X) and powder, trypsin-EDTA (0.5%, 10X), and Hank's Balanced Salt Solution (HBSS, 1X) were provided by Gibco (NY, USA). Endothelial cell growth medium 2 and SupplementMix were from PromoCell (Heidelberg, Germany). PrestoBlueTM cell viability reagent and LIVE/DEADTM viability/cytotoxicity kit were from Invitrogen by ThermoFisher Scientific (OR, USA). Cell

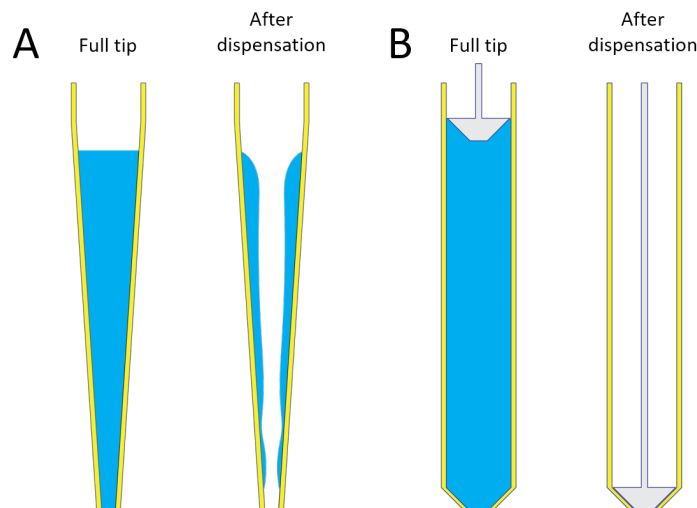


Figure 2.1: Standard (A) and positive displacement (B) pipettes compared: when dispensing special liquids, such as high viscosity gels, standard pipettes dispense less than the full volume. Positive displacement pipettes instead deliver the full volume thanks to the tight piston pushing the liquid all the way through.

culture flasks (75 cm², Corning, NY, USA) and polystyrene 6-well tissue culture-treated plates (Falcon, NC, USA) were used to culture cells.

2.1.5 Characterization instruments

The tools and instruments used for the measurements and analysis of the data in this work are the following: an inverted fluorescence microscope, Axio Observer V (Zeiss, Germany), was used for monitoring the chip operation and acquiring images of the bead samples. A mechanical testing column, the 5943 Instron Universal Testing System (Instron, MA, USA) was used for the compression and tensile tests. A rheometer, the MCR 302 by Anton Paar (Austria), was used for the rheology studies. Confocal microscopy was performed using the Leica SP5 Blue, by Leica (Germany), gently provided by the Advanced Light Microscopy/ Spectroscopy laboratory at CNSI. Each instrument was operated using the standard software provided by the manufacturer. Nanoindentation studies were performed using an Atomic Force Microscope, the BioScope Catalyst AFM (Bruker, CA, USA), on which a silicone nitride cantilever with an affixed polystyrene bead as tip (diameter 2.5 μm) was mounted as probe (Novascan, IA, USA), with a spring constant of 0.01 N m^{-1} . The cell metabolic activity was measured using a BioTek UV/vis Synergy 2 (VT, USA) microplate reader. Data were analyzed using different softwares: pore size analysis was performed using a MATLAB 2016a script (Mathworks, MA, USA), temperature stability and shrinking-swelling studies were performed using FIJI [26], the same was used for image processing, 3D reconstructions and cell counting.

2.2 Methods

In this section the procedures and protocols followed when performing the experiments are described.

2.2.1 Fabrication of the microfluidic device

A flow-focus device was fabricated using soft lithography. Briefly, 4 inch mechanical grade silicon wafers were coated with 80 μm and 70 μm layers of negative photoresist (KMPR 1050) and patterned in sequence using standard photolithography [7]. The PDMS base and the curing agent were mixed at a ratio of 10 to 1, poured onto the molds in petri dishes, degassed in a vacuum chamber, and cured in an oven at 65 $^{\circ}\text{C}$ for >4 h. The PDMS device was peeled from the mold and punched with 0.8 mm holes at the inlets and outlets. Devices and glass slides were then activated via air plasma (Plasma Cleaner, Harrick Plasma, NY, USA) and bonded together to enclose the microchannels. The devices were then treated with Aquapel by flushing the channels with the solution and subsequently washed with Novec 7500 oil, to make channel surfaces fluorophilic.

2.2.2 Gelatin methacryloyl synthesis

GelMA with a high degree of methacryloyl substitution was synthesized according to previous publications [36]. Briefly, DPBS (100 mL) was heated to 50 $^{\circ}\text{C}$ to dissolve the gelatin (10 g) to yield a 10% w/v solution. While stirring at 240 rpm, MA (8 mL) was added to the gelatin solution dropwise, resulting in a turbid mixture, which was stirred for 2 h at 50 $^{\circ}\text{C}$. This condition was particularly chosen to prevent the hydrolysis of the proteins in gelatin [32]. To stop the reaction, fresh DPBS was added to the reaction mixture, followed by dialysis using 12 kDa to 14 kDa molecular weight cutoff (MWCO) membranes. This was performed by submerging the dialysis bags in DI water continuously stirred at 300 rpm and heated at 40 $^{\circ}\text{C}$, for at least seven days in order to remove unreacted methacrylic acid and other impurities. A clear solution was obtained after dialysis, which was lyophilized using the freeze dryer, yielding white solid GelMA foam. The dry GelMA tubes have a shelf life of several months when stored in a dry environment.

2.2.3 Bulk GelMA scaffolds fabrication

A 0.5% w/v solution of Irgacure in DPBS was prepared by mixing 25 mg of photoinitiator in 5 mL of buffer solution, followed by stirring and heating for about 20 min at 80 $^{\circ}\text{C}$. Once the PI had dissolved, dry GelMA was added to obtain the desired hydrogel concentration and the solution was again heated to 80 $^{\circ}\text{C}$ for 30 min. The GelMA warm solution was then filtered using the syringe filter to remove any debris or contaminant. It was important to remark that, prior to utilization, the GelMA solution with photoinitiator was light sensitive and therefore it must be stored in dark containers. To obtain a uniform thickness for all samples, a specific crosslinking setup was been designed: two stacks of microscope glass cover slips were placed over each side of a microscope slide as spacers, the number of slips defines the thickness in multiples of 100 μm . Then, a defined amount of liquid GelMA was pipetted in the space in between the cover slip stacks, the volumes used depend on the desired sample dimensions. Finally the droplet was leveled with respect to the spacers using another cover slip. In this case, rectangular samples of ~ 25 mm length, ~ 10 mm to 20 mm width and ~ 0.3 mm to 1 mm thickness, depending on the application. The sample was then crosslinked using the UV curing system described in the previous section: the exposure to UV (360 nm to 480 nm) was performed at an intensity of

10 mW cm^{-2} for 1, 2 or 3 min, yielding bulk gel samples that were later punched, for compression tests and cell studies, or cut for tensile tests

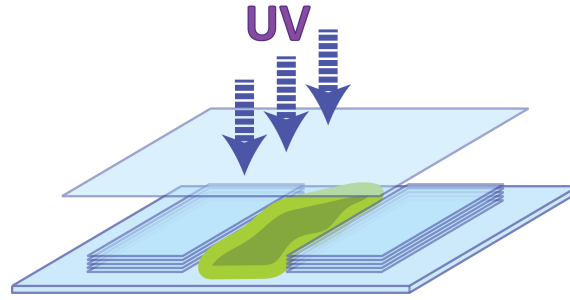


Figure 2.2: Schematic drawing illustrating the crosslinking setup. Pressing the top slide allows the creation of highly uniform samples for repeatable measurements.

2.2.4 GelMA bead fabrication

10 mL of 0.5 % solution of surfactant in oil was made by mixing 1 mL of Pico-Surf 5 % in 9 mL of Novec7500. A solution of GelMA and photoinitiator was prepared as indicated in the previous paragraph. Both solutions were loaded into syringes and mounted on two separate syringe pumps. TYGON[®] tubing was used to connect the syringes to the microfluidic device: to plug into the 0.8 mm punched holes short cuts of PEEK tubing were used to lower the flow resistance and therefore reduce the chances of leakage from the inlets. Consequently the TYGON[®] tubing was directly plugged into the outlet of the device, pouring the outflow in a replaceable microcentrifuge microtube. Then the flow rates were set for each syringe pump in order to obtain the desired microbead size and finally the pumps were activated, starting with the syringe containing oil and following with the GelMA one. It is important to maintain the GelMA syringe and the relative tubing at $\sim 37^\circ\text{C}$ in order to lower the viscosity of the gel, especially if high in concentration, else clogging might occur in the microfluidic chip. Care must be taken not to raise also the temperature of the chip and therefore of the oil: this would make the oil/water phase interface unstable because of the thermal energy acting on the surfactant. The operation of the microfluidic chip was constantly monitored using the inverted optical microscope. Depending on the GelMA flow rate, the Eppendorf tubes were periodically replaced to obtain well defined volumes of beads per each container. The full tubes then were stored in a 4°C fridge to preserve the spherical shape of the beads.

2.2.5 GelMA beads handling protocol

The GelMA microbeads were processed following a novel procedure, exploiting the temperature dependence of the hydrogel's viscosity. The microbeads and the solutions used for processing were constantly kept at 4°C using an ice bath. A 20 % v/v solution of perfluorooctanol in Novec 7500 was prepared and cooled down along with a 0.5 % solution of PI in DPBS. The microbeads suspension was centrifuged for 10s and the oil was pipetted out from the bottom of the tube, since it is the heaviest. The PFO solution was then mixed with the microspheres in equal volume,

in order to break down the emulsion and remove the surfactant from the microbeads' surface. The Eppendorf tubes were agitated for few seconds, let to rest for 3 min, centrifuged again for 10s and finally the PFO solution was pipetted away. Then, the PI solution was added, in a 1:1 ratio with respect to the volume of beads, then the tubes were shaken and centrifuged as before and finally the remaining oil was removed from the bottom and the excess DPBS was taken away from the top. The concentrated suspension was withdrawn with the positive displacement pipette and placed onto the crosslinking setup introduced in section 2.2.3.

Non-annealed crosslinked microbead samples, that are isolated GelMA beads, can be obtained by crosslinking a small volume of highly diluted suspension on a regular microscope glass slide. The beads can then be stored in a centrifuge tube and shaken for 10s to obtain separate microspheres.

2.2.6 Pore size measurement

In order to visualize the interstitial voids in between the beads, various beaded GelMA samples (several copies for each exposure time) were incubated in a DI water/based 15 mmol solution of fluorescein isothiocyanate-dextran for at least 30 min. The samples were then placed on a microscope cover slip, kept hydrated using the same fluorescent solution and imaged using the confocal microscope. For each sample about 100 z-slices were captured, each with a voxel depth of 1.3 μm , pinhole diameter of 20 μm and Green Fluorescent Protein (GFP) filtering as setting. Void fraction and pore size were automatically analyzed using a MATLAB script: to obtain the first, the total pore volume was calculated by summing up the pore area (in pixels) for each Z-slice to then multiply the result times the volume of a single voxel (11.7 μm^2). The ratio between whole sample and total pore volume was finally calculated. The median pore diameter was obtained using several slices and evaluating the area of each interconnected pore to then derive the diameter of the relative equivalent circle.

2.2.7 Mechanical analysis

The mechanical analysis was performed on bulk and beaded GelMA samples crosslinked for 1, 2, 3 min, using the Instron testing system with a 100 N load cell mounted. Samples were always incubated in DPBS for 1 h before testing. Compression measures were performed on samples of 8 mm diameter and 1 mm thickness, obtained using proper spacers and a puncher. The tests were performed with a compression rate of 1 mm s^{-1} and stopped at a strain of 0.3. The region from 0 to 0.1 strain was linearly interpolated to obtain the Young compression moduli.

Tensile tests were performed by cutting the crosslinked samples into rectangles, with size 10 mm x 15 mm x 1 mm. These were then glued to a paper holder using a common cyanoacrylate-based glue, such as Krazy Glue. Given the large difference in magnitude of both hardened glue and paper, such setup can be considered reliable for measuring the Young tensile moduli of the hydrogels. The paper holders were clamped to the Instron test grips and the experiment was performed at a rate of 10 mm s^{-1} . The slope of the linear stress-strain region at strain <10% provides the tensile modulus.

Image 2.3 shows the two measuring setups used.

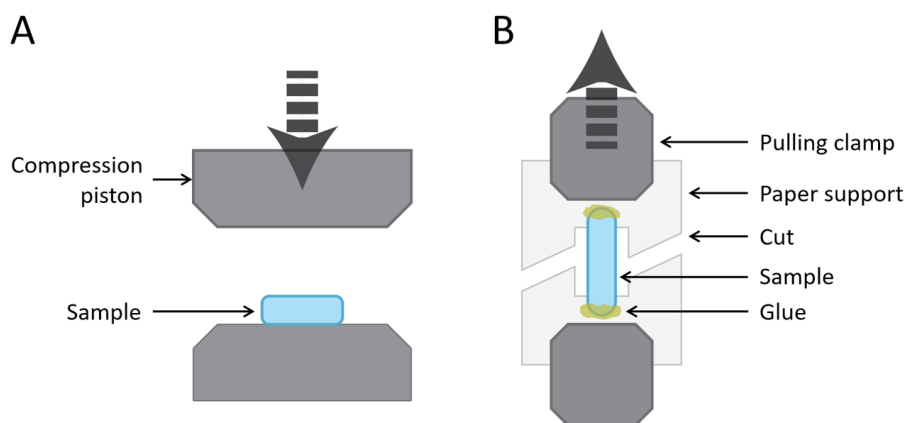


Figure 2.3: Mechanical characterization setups using the Instron testing column: (A) Compression, (B) Tensile.

2.2.8 Rheology studies

Oscillatory shear rheology was conducted using the MCR 302 Rheometer to characterize the rheological properties of the gels. The machine setup consists of a parallel plate geometry, with a sandblasted measuring plate and 8mm rotating probe (PP08/S), then the calibration was performed and the samples were loaded one by one. To obtain the viscoelastic moduli, an oscillatory frequency sweep was performed at 0.1 rad s^{-1} to 100 rad s^{-1} under a small oscillatory strain of 0.1 %, all in the linear viscoelastic region at 25°C , obtaining the viscoelastic moduli vs angular frequency. The samples were hydrated during the experiments thanks to a controlled environment chamber provided by the manufacturer.

2.2.9 Temperature stability studies

The temperature stability studies of non-crosslinked beads after performed following the washing step, as described in section 2.2.6, then transferring them into closed tubes containing DPBS+PI solutions at different temperatures: the 37°C suspension was kept in the cell incubator, the 4°C suspension was kept in a monitored ice bath and the room temperature sample was kept in a ventilated open environment. The analysis on crosslinked beads was done washing the individual microspheres and exposing them to UV (120 s at 10 mW cm^{-2}), as described in section 2.2.6. They were then transferred into a 37°C PBS+PI solution, to verify the bead stability in an cell incubation environment.

Images of the samples were captured at predetermined timepoints, pipetting $20 \mu\text{L}$ of suspension on glass slides and imaging using brightfield microscopy. The size variation, that is the swelling in this case, was measured using the ImageJ software: in depth, the images were thresholded in order to highlight only the edges of the separate beads, obtaining a binarized black&white image. Then, the function “Fill holes” was used to obtain full circles out of the rings created from the bead edges. Following, the “Watershed” function was used to separate the beads that were in contact with each other. Finally the “Analyze particles” function was used to automatically find and measure the bead areas with the help of some parameters set by the user such as circularity, set to 0.95 (out of 1) to filter out broken and deformed beads, and size, set in a range of $90 \mu\text{m}^2$ to $150 \mu\text{m}^2$. Once all the areas were eval-

uated, the equivalent diameter was extracted by inverting the circle area formula. Figure 2.4 shows the different steps of the algorithm.

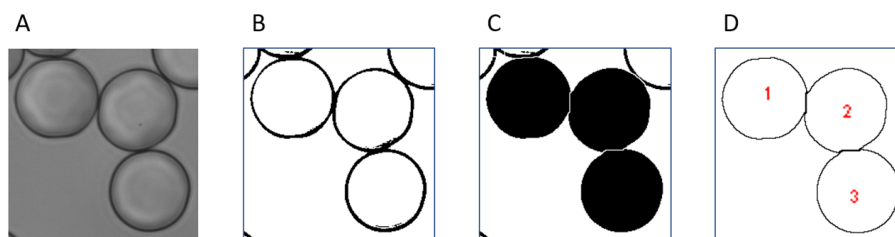


Figure 2.4: Pictures illustrating the algorithm used to automatically measure the equivalent diameters of the beads when imaged using brightfield microscopy: (A) Original image in grayscale, (B) Thresholded image, (C) Bead filling and Watershed algorithm application, (D) Identified bead edges.

2.2.10 Swelling and shrinking analysis

The swelling and shrinking studies on non-annealed beads, either in their gel form or crosslinked for 120s, were performed starting from a DPBS dilute dispersion of beads kept at 4 °C. Swelling studies were performed by dispersing the beads in deionized water, while the shrinking studies were performed in 5X DPBS.

The studies on non-crosslinked beads were performed at 4 °C: in this case the initial timepoint coincides with the end of the washing step, that is the oil removal. The crosslinked microspheres were analyzed while incubated at 37 °C, simulating the cell culturing environment conditions. The beads, dispersed in DPBS, were crosslinked after the cleaning process and incubated in the designated solutions.

The samples were imaged at predefined timepoints using brightfield microscopy and the size was measured following the same method described in the previous section.

2.2.11 Atomic Force Microscopy indentation studies

An Atomic Force Microscope was used to evaluate the Young modulus of single microbeads and their bulk equivalents. The machine used, a BioScope Catalyst AFM, was jointly equipped with the Zeiss LSM 5 confocal microscope, improving the tip positioning accuracy. The samples, individually crosslinked microbeads and bulk GelMA gels, were glued on glass slides using the Cell-Tak tissue adhesive and later submerged in DPBS, along with the probe cantilever, ready for the measurements. As specified in the Materials section, the probe tip consists of a microsphere, in order to avoid penetration into the surface of the sample. Therefore, the measurements were carried out with a 100 nm indentation, calculating the compression moduli using the Hertz mechanical contact model commonly used for spherical probes [16]. 3 samples per condition were analyzed: for the case of microbeads, at least 5 beads per sample were considered, each was characterized 5 times, totaling 25 measures per sample. Bulk GelMA samples were studied in the same fashion, 5 positions 5 times each for a cumulative of 25 measures per sample.

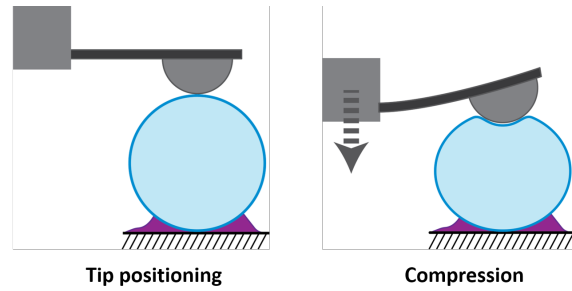


Figure 2.5: Pictures illustrating the AFM tip morphology and operation when used in tapping mode to evaluate the Young compression modulus of a single GelMA microbead.

2.2.12 Cell culture

Cells were cultured in dedicated flasks, under a 5% CO₂ atmosphere at 37°C in a regular cell culture incubator. NIH/3T3 fibroblasts were cultured in Dulbecco's Modified Eagle's Medium (DMEM), supplemented with 10% Fetal Bovine Serum (FBS) and Penicillin/Streptomycin antibiotics (P/S), cell passaging was performed approximately twice a week. Immortalized human umbilical vein endothelial cells (HUVECs) were cultured in endothelial growth medium 2, mixed with Supplement-Mix and P/S. Cell medium was replaced every 2 or 3 days for both cultures, while also checking cell adhesion to the flask as an indicator of cell health. HUVEC and 3T3 cells were then withdrawn to perform the experiments using 0.5% trypsin-EDTA, followed by counting using a hemocytometer and resuspension either in the media (for cell migration tests), GelMA solution (for bulk encapsulation), or cooled, and therefore physically-crosslinked, bead suspension (for encapsulation in beaded GelMA scaffolds).

2.2.13 3D cell encapsulation

Cell-loaded scaffolds of bulk and beaded GelMA were prepared by taking 20 µL of NIH/3T3 fibroblasts cell suspension, with a density of 10⁶ in 1 mL of DMEM dispersion medium, mixed either with 80 µL of GelMA (~25%), obtaining an hydrogel a final concentration of ~20% or, in the other case, mixed with 80 µL of concentrated bead suspension (~45 × 10⁴ beads per mL) in DPBS with 0.5% PI. The cell/GelMA (beads or bulk) volume was then crosslinked using the previously described setup: UV intensity was set to 10 mW cm⁻² and exposure time was 120 s, obtaining samples of ~10 mm in diameter and ~0.3 mm thickness. Thin samples were preferred in order to facilitate imaging using fluorescence and confocal microscopy. Each sample, having ~5 × 10⁵ cells encapsulated inside, was gently washed with warm DPBS (37°C) to remove non-crosslinked GelMA or non-annealed microbeads and surface cells. Finally the samples were transferred to 6-wells plates and cultured in media for up to 14 days, with periodic media changes every 48 h. Multiple samples, with at least 3 replicates per timepoint, were then imaged after staining at predefined intervals using the fluorescence microscope.

2.2.14 Metabolic activity assessment

The cellular metabolic activity in cell-encapsulating samples was measured on day 1, 3, 5, 7 and 14, using the PrestoBlueTM assay. The measure was performed using the manufacturer protocol [22]: the results were obtained using the microplate reader BioTek and the values were corrected with respect to the background signal of the PrestoBlueTM-containing media without cells.

2.2.15 3D cell migration

Bulk and beaded GelMA samples were prepared using the standard procedure illustrated previously: cylinders with ~ 10 mm diameter and ~ 0.3 mm thickness, 10 mW cm^{-2} were UV exposed for 120 s and punched. Then $50 \mu\text{L}$ of cell suspension (1×10^6 cells per mL) were gently pipetted onto the samples: some were immediately imaged while others were analyzed at different timepoints. To facilitate the operation, thick PDMS molds were used to confine the volume around the cylinders and simplify pipetting. Imaging was performed using confocal microscopy, capturing ~ 180 slices starting from the bottom.

2.2.16 Live/Dead assay

Cell viability in the hydrogel samples was assessed using a Live/Dead assay: the hydrogels were incubated for 20 minutes using 1 mL of staining solution prepared by adding $20 \mu\text{L}$ of ethidium homodimer-1 and $5 \mu\text{L}$ of calcein AM to 10 mL of DPBS. Imaging was performed using the fluorescence microscope at excitation/emission wavelengths $494/515 \text{ nm}$ for calcein and $528/617 \text{ nm}$ for ethidium homodimer-1. It is important to note that this staining kills cells and therefore samples must be disposed of once imaged. Live and dead cell counting was performed using the functions provided by ImageJ: the images were split in separate channels and therefore dyes, then each was thresholded to highlight only the bright cells, aggregates were broken into different parts using the "Watershed" function and finally the "Analyze particles" command is used to count the cells.

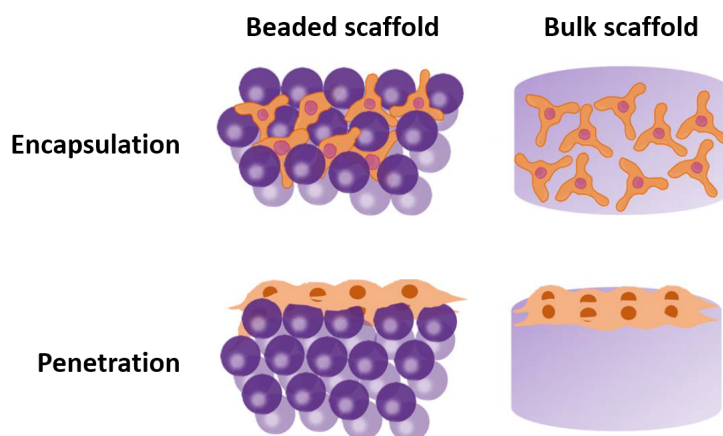


Figure 2.6: Schematic of the cell experiments to be performed on the scaffolds.

Chapter 3

Results and discussion

In the following chapter, the main results are shown and analyzed.

3.1 GelMA bead fabrication

The flow focus microfluidic droplet generating device is able to produce microbeads of tunable size, operating on a wide range of concentrations of GelMA solutions. Tuning the ratio between GelMA and oil flow rates, it is possible to obtain different bead diameters: in this case the GelMA flow rate is kept constant while sweeping the oil flow rate. The microfluidic system can deliver highly uniform bead sizes, tunable with high accuracy within the resolution of the syringe actuators, and with fabrication rates reaching up to 45000 microbeads per minute when using low-viscosity polymer solutions. At higher concentrations, and therefore higher viscosity, the water phase flow rates must be reduced to avoid pressure build-up in the microchannels. Another side effect is the difficulty in generating larger GelMA beads: when using highly viscous solutions, the oil flow rates must be high enough to pinch the other flow, making it difficult to achieve large microbeads.

An approach to improve the system's performance is to lower the viscosity of thermally-responsive polymers such as GelMA: warming up both syringe and tubing, it is possible to achieve sizes similar to the ones obtainable using lower polymer concentrations. In this case the temperature of the solutions was regulated to $\sim 37^\circ\text{C}$ using an incubator.

It is possible to achieve bead sizes within the ranges of $75\ \mu\text{m}$ to $115\ \mu\text{m}$, $70\ \mu\text{m}$ to $110\ \mu\text{m}$ and $75\ \mu\text{m}$ to $105\ \mu\text{m}$ using 7%, 10% and 20% GelMA solutions respectively. The worst case Coefficient of Variation (CV) is 0.33, when using high viscosity liquids, indicating a highly uniform size distribution. The bead fabrication rate can be easily derived for each condition dividing the flow rate by the single bead volume. A thorough study on the performance of the microfluidic droplet generation device has been carried and the results are displayed in Figure 3.1.

The water phase flow rates are fixed for each polymer concentration: the 7%, 10% and 20% solutions flow at 10 , 4 and $0.5\ \mu\text{L}\ \text{min}^{-1}$ respectively.

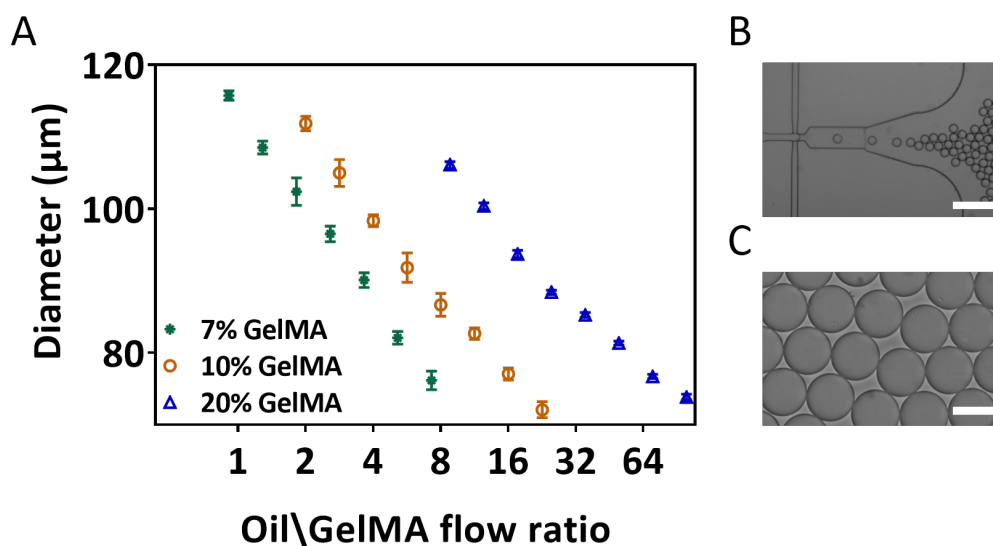


Figure 3.1: (A) Plot showing the versatility of the flow-focus droplet generation device, generating beads with diameter from circa 70 μm to 120 μm by altering the flow ratio, (B) Picture of the device in operation, scale bar indicates 500 μm , (C) GelMA microbeads in oil, scale bar indicates 100 μm

3.2 Microbead processing and scaffold fabrication

The microbeads were processed following the procedure described in section 2.2.5. The newly designed cleaning protocol preserves the spherical shape, apart from a fraction of the beads ($< \sim 1\%$) that got damaged (broken, deformed) because of the handling, probably when pipetting and centrifuging. The protocol is therefore efficient in cleaning the microbeads from the oil, without the use of any chemical reaction but only exploiting physical crosslinking, leveraging therefore the temperature sensitivity of GelMA.

Some phenomena are worth noticing during these steps, a first example is the change in size when cleaning the emulsion from the oil: when dispersed in the PBS+PI solution, the beads are noticeably larger, showing a $\sim 30\%$ increase in diameter. This can be attributed to the change in interfacial forces between the GelMA solution forming the bead and the surrounding liquid, enhanced by the removal of the surfactant covering the bead surface. Another cause of swelling is also the diffusion of PBS into the bead because of osmotic pressure. UV-mediated crosslinking further changes the size of the microbeads, these in fact shrink by $\sim 20\%$ in diameter after exposure in the PBS+PI solution. This behavior can be explained by considering the crosslinking mechanics: in fact the inter-chain linkage obtained when the photoinitiator is activated “pulls” the polymeric chains closer to each other, reducing therefore the total volume of the bead. Another effect due to crosslinking is the formation of certain patterns on the single beads: because of the light scattering through the water phase, some lines appear in the microbeads. Moreover, some circular traces might appear when beads are laying over others, acting as lenses. This phenomenon is easily observable when crosslinking single beads and dispersing them in PBS

Following the method illustrated in section 2.2.3 and using a highly dense suspension

of microbeads in PBS+PI, it is possible to obtain highly annealed microstructures that result to be stiff and interestingly, self-standing. The beaded GelMA scaffolds can withstand immersion in cell media and incubation for more than 14 days, making them a promising support for 3D cell cultures.

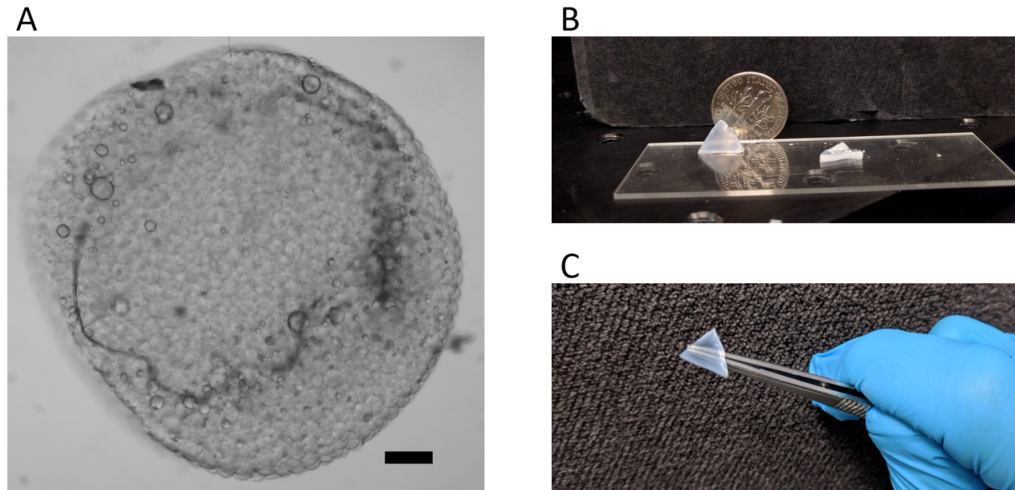


Figure 3.2: Beaded scaffold pictures showing: (A) Brightfield microscopy image, (B) Self-standing structure and shape, (C) Ease of handling. Scale bar indicates 250 μm

3.3 Temperature stability studies

The temperature stability studies are carried on individual beads both UV-crosslinked and non-crosslinked, as described in the methods section 2.2.9. The length of the experiments is chosen depending on the behavior in each condition. This experiment is needed to verify the stability of the beads during the handling steps, when they are physically crosslinked and transferred to an aqueous solution. The chemically crosslinked samples were tested under incubation conditions (at 37 °C), to verify their compatibility with cell culture protocols. From the data acquired, it can be seen that physically crosslinked beads are stable for up to 6 h when stored in a 4 °C suspension, while after 12 h their diameters increase by circa 15 % due to swelling. Beads stored at room temperature start increasing their volume after 3 min, indicating their high susceptibility to warmer temperatures. After 10 min, 30 min and 1 h the diameters are circa 7 %, 20 % and 50 % larger, respectively. At the last timepoint the beads are hardly distinguishable from the background because of the very high swelling. As expected, the non-crosslinked beads can withstand higher temperatures for even shorter times: at 37 °C the beads are stable for a single minute, after which they rapidly swell and then dissolve in the suspending solution.

Meanwhile, chemically crosslinked beads show a very high stability at cell incubation temperature, 37 °C: after a 24 hours monitoring period, the diameter variation of the microbeads is not significant, staying almost constant over the entire experiment. This property makes the GelMA microbeads compatible with the cell culturing environment and therefore also suitable for the fabrication of 3D scaffolds for tissue engineering.

Figure 3.3 provides a summary of the results obtained in this experiment.

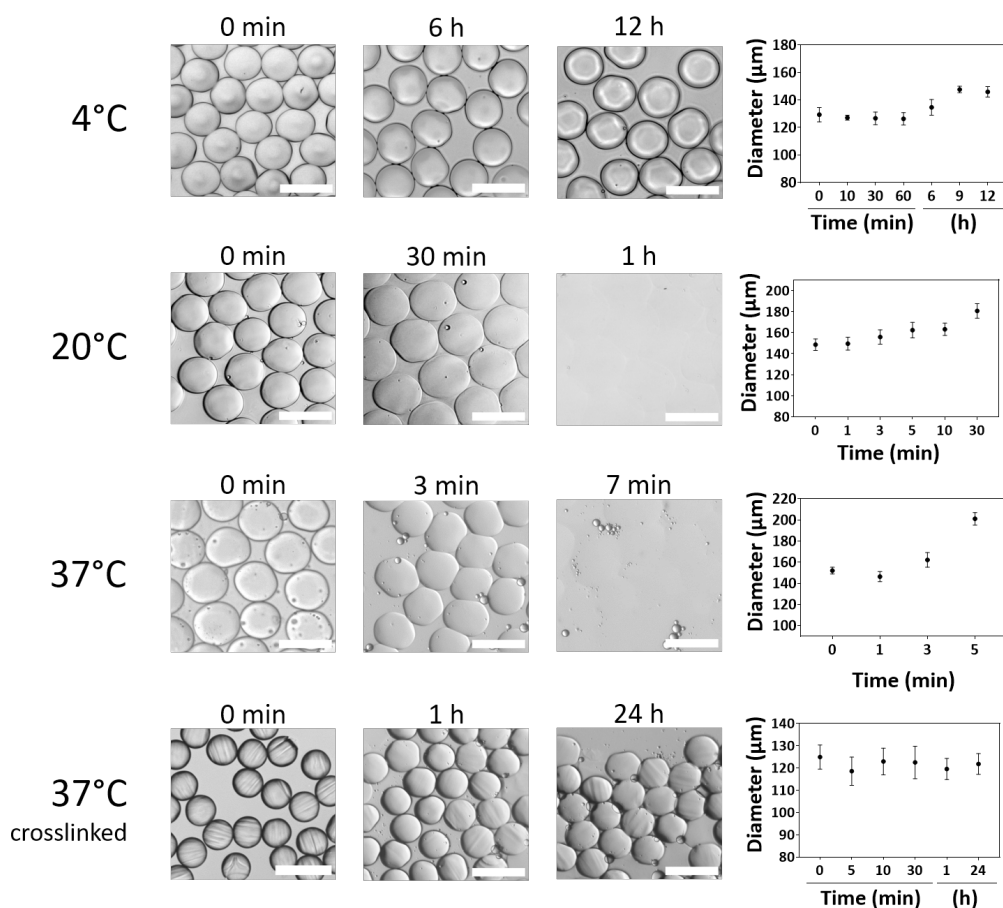


Figure 3.3: Table summarizing the results of the temperature stability studies. The pictures are a sample of those used for deriving the data plotted on the side. Scale bars indicate 200 μm

3.4 Swelling and shrinking studies

Crosslinked and non-crosslinked beads are then considered for studies on their swelling and shrinking behaviors in water with different ionic concentrations. To do so, beads are immersed in specifically formulated solutions as indicated in section 2.2.10. After observing the behavior of the beads in previous trials, the measurements on non-crosslinked beads are carried on a span of time up to 20 min since the bead size would be stable thereafter. For similar reasons, the crosslinked beads are monitored for 120 minutes.

As expected, for both bead conditions there is a change in volume depending on the surrounding solution: non-crosslinked beads react faster and in larger magnitude, swelling up to 10 % and shrinking up to 4 %, because of the high degree of freedom of the polymer chains that can easily absorb or expel the water molecules surrounding them. Crosslinked microbeads are instead more stable, as expected, for the opposite reason: polymer chains are tightly bound to each other by the photoinitiator, making the beads less susceptible to water transfer due to osmotic pressure. Figure 3.4 and 3.5 display images of the beads before and after the predetermined incubation times, either in deionized water or 5X PBS. The change in volume is hardly evaluated by eye, the results are therefore obtained through image processing using

ImageJ. The crosslinked beads instead did not either shrink or swell in a significant manner: a small and random population of beads did experience a change in volume in both cases, probably because of partial crosslinking, but the largest part has slight variations in size, negligible with respect to their diameter.

This experiment shows how stable these beads are in different immersion solutions, ranging from deionized water to 5X phosphate buffer solution. Such property makes the microbeads a reliable building block for the fabrication of scaffolds for 3D cell cultures, to be therefore soaked in a wide variety of cell culture media.

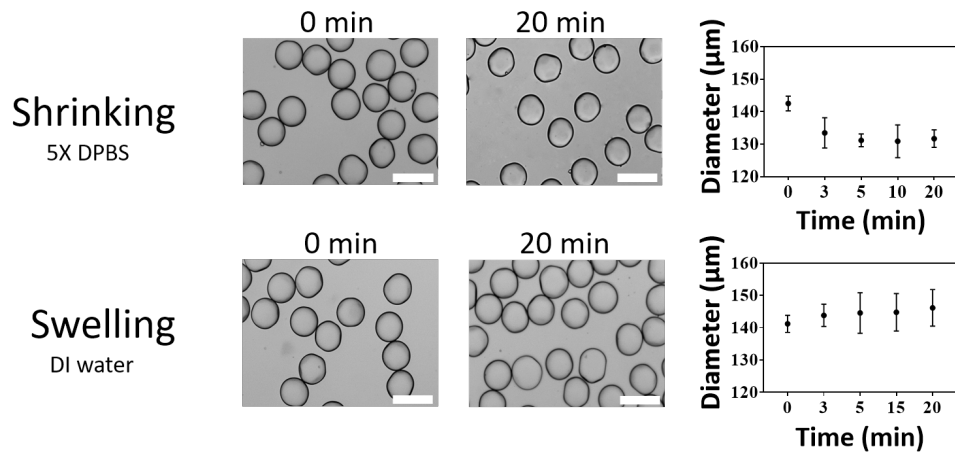


Figure 3.4: Shrinking and swelling behaviors of non-crosslinked GelMA microbeads immersed in hypertonic or hypotonic solutions, scale bars indicate 200 µm.

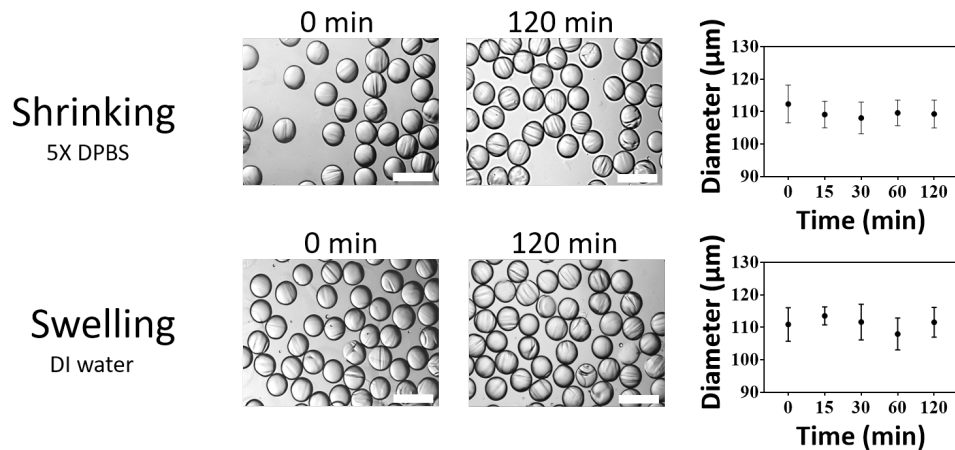


Figure 3.5: Shrinking and swelling behaviors of individually crosslinked GelMA microbeads immersed in hypertonic or hypotonic solutions, scale bars indicate 200 µm.

3.5 Pore size characterization

Porosity is one of the main characteristics that are crucial for the development of novel scaffolds for 3D cell culturing: pore size, shape, density and hierarchy are factors that influence how cells organize in space, receive nutrients, communicate with

each other, grow and also mutate or differentiate in specific cases [8]. Given the spherical shape of the microbeads, these organize themselves in opal-like structures where each bead is touching the surrounding ones ideally through single contact points. An entire branch of geometry, pioneered by mathematicians such as Gauss, is dedicated to the sphere packing problem but is out of the scope of this work. In brief words, a wide range of different pore types (both in size and shape) are formed in between the beads: their size depends on different factors such as bead diameter and organization in space. The smallest achievable pore size can be obtained when the beads are organized in a close-packed geometry, in that case pores occupy 26 % of the whole volume [14].

Following the technique described in section 2.2.6, it is possible to evaluate the porosity of the scaffolds using confocal microscopy and a fluorescent dye to then conduct the equivalent of a tomographic study of the structure. Circa 100 Z-slices are acquired, from these a 3D reconstruction can be obtained using ImageJ, an example is displayed in figure 3.6.

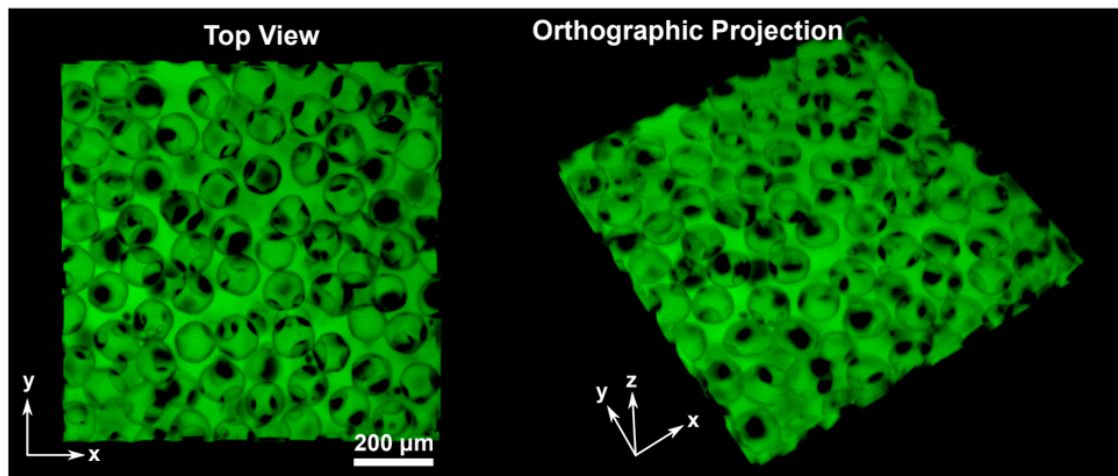


Figure 3.6: Top and orthographic views of the 3D reconstruction of the porous architecture of the beaded GelMA scaffolds. The voids represent the spaces occupied by microbeads while pores are represented by the green-dyed structures. The sample consists of 20 % GelMA beads annealed for 120 s.

The reconstructed geometry shows that the scaffolds have a highly interconnected porous structure, facilitated by the loose packing geometry: it is experimentally proven that the packing density is strongly dependent on the time between mold filling and annealing [27]. In fact, a longer time between the two sample fabrication steps allows the microbeads to move and settle into more stable positions, with the final goal to get a close-packed overall geometry. Therefore, to achieve results as uniform and meaningful as possible, the time between mold filling and UV-annealing is kept constant throughout the experiment to 60 s.

One of the main hypotheses formulated in this work is that the porosity of beaded GelMA scaffolds could be independent on the structure's stiffness, that in this case is a function of the UV exposure time. To prove such claim, a custom MATLAB script is used to evaluate void fraction and pore size distribution throughout the samples' thickness, as described in section 2.2.6. Results are displayed in figure 3.7. Given the results obtained, several conclusions can be derived: as hypothesized the

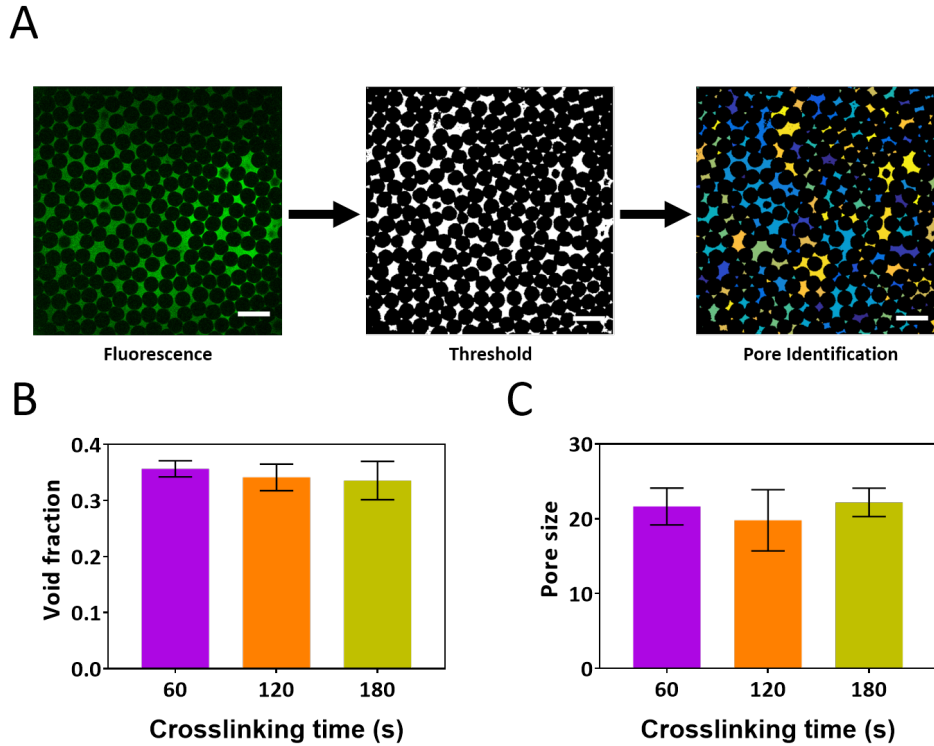


Figure 3.7: (A) Extract from the pore analysis script showing how each slice is processed, interconnected pore areas are tagged and their areas evaluated to finally calculate void fraction and median pore size, (B) Void fraction at different scaffold annealing times, (C) Median pore size for the same scaffolds. Scale bars indicate 250 μm

pore size is independent from the stiffness of any beaded GelMA scaffold, that is the opposite behavior with respect to bulk scaffolds. Moreover, the void fraction amounts to circa 35 % of the total sample volume, indicating that the microbead packing is not the most efficient, as expected. Finally the equivalent pore diameters show a distribution towards the smaller values as expected, this is due to the geometry of the structure.

It is intuitive that pore size can be easily controlled by tuning the microbead sizes: smaller diameters will induce smaller pores. However to keep the same stiffness among samples made of various bead diameters, UV exposure times should be properly tuned for each condition. Gradients of porosity can also be obtained by properly laying different layers of beads of varying sizes, this would allow the design of biomimetic structures inspired by tissues present in bones, brain and other organs.

3.6 Mechanical characterization

In this section, different mechanical properties of the annealed and non-annealed beaded GelMA samples are described and compared with their bulk counterparts. The methods are described in the relative sections in the previous chapter.

3.6.1 Compression

The compression moduli of the beaded and bulk GelMA samples are evaluated: it is expected that the microbead-based scaffolds will exhibit a slightly lower Young modulus because of the high macroporosity and the weak interconnecting forces holding the microspheres together. Obviously, it is also expected that stiffness will increase with exposure time.

The results of the measurements are displayed in figure 3.8.

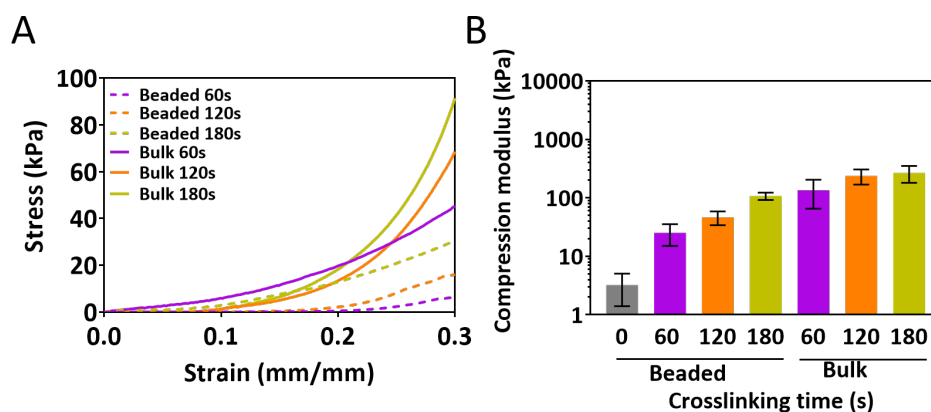


Figure 3.8: (A) Curves displaying the compressive stress vs strain behavior of beaded and bulk GelMA scaffolds crosslinked for 60, 120 and 180 s. (B) Logarithmic plot of the compression moduli derived from the stress vs strain curves.

The results indicate that the beaded GelMA scaffolds have stiffnesses of 25, 46 and 107 kPa for 60, 120 and 180 s of exposure to UV radiation, while bulk samples exhibit stiffnesses of 140, 210 and 260 kPa with the same crosslinking conditions. As expected, the stiffness of the beaded samples is a fraction of their bulk counterpart. This is due to the presence of a large porous network and the weak interconnecting forces between the microbeads. Obviously, it is possible to obtain higher moduli with longer exposure times, obtaining scaffolds of stiffness directly comparable with the one characterizing osseous tissues. Nevertheless such exposure times would preclude the presence of cells in the scaffold prior to crosslinking due to the toxicity of prolonged UV exposure, a hurdle that can be overcome by using visible light crosslinking, a more cell-friendly technique requiring another photoinitiator. Another approach to increase the stiffness can also be further increasing the polymer concentration, with the risk of clogging the microfluidic device, or reducing the microbead size, obtaining smaller pores.

3.6.2 Tensile

Then, the tensile moduli are measured using the same conditions as in the previous section. In this case the difference in moduli is expected to be larger than the previous case since the beaded structure is held together solely thanks to the binding forces between microspheres, enabled during the annealing process. Bulk GelMA samples instead keep their shape thanks to the dense network of polymeric chains bound to each other through the activated photoinitiator.

As expected, the results show a noticeable difference in tensile moduli between the

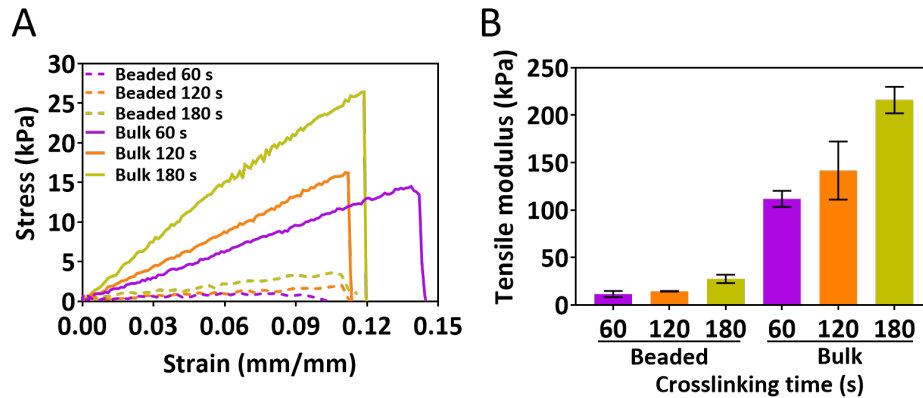


Figure 3.9: (A) Curves displaying the tensile stress vs strain behavior of beaded and bulk GelMA samples annealed, and therefore crosslinked, for 60, 120, 180 s. (B) Tensile moduli derived from the stress vs strain curves.

two sample types: beaded GelMA samples have moduli up to 10 times smaller with respect to their bulk counterparts. For crosslinking times of 60, 120, 180 s the annealed microbead-based scaffolds exhibit elastic moduli of 10, 15, 30 kPa circa while the others have 100, 150, 200 kPa moduli. It can intuitively be deduced that scaffold fabricated with smaller bead size will achieve higher tensile moduli, getting closer and closer to the bulk GelMA performances, thanks to the load distribution on the increased number of internal contact points.

An interesting property that can be deduced from Figure 3.9(A) is that both types of scaffold share similar fracture strains at around 12%, while the fracture strengths differ by at least one order of magnitude. This means to obtain the same elongation as their bulk counterparts, beaded scaffolds need smaller forces while sharing the same maximum strain limits.

3.6.3 AFM

To verify that the properties of beaded GelMA scaffolds derive from the novel macroscopic morphology (that is in this case the opal-like geometry) and not from different material properties, the stiffness of individually crosslinked beads is evaluated. Given the microscopic size of each GelMA microbead, the mechanical testing tower must be replaced by a much more sensitive device, both in positioning and force: the ideal candidate in this case is the Atomic Force Microscope, one of the most versatile instruments for characterizations at the micro and nanoscale. Moreover, the microbead stiffness is also an important parameter defining the behavior, such as adhesion or penetration, of cells growing in the porous micro-environment. As described in section 2.2.11, the individual beads are glued to a rigid substrate and indented with the AFM spherical tip. Bulk GelMA samples are also analyzed with the same procedure. The results are displayed in figure 3.10

The plots show, as expected, that the individual microbeads have the same compression Young moduli as their bulk analogues: in both cases the stiffness values amount to circa 120, 200, 230 kPa. It can be deduced then that the microbead fabrication, cleaning and annealing processes do not alter the physical properties of the material, making it easier to predict what will be the mechanical interaction

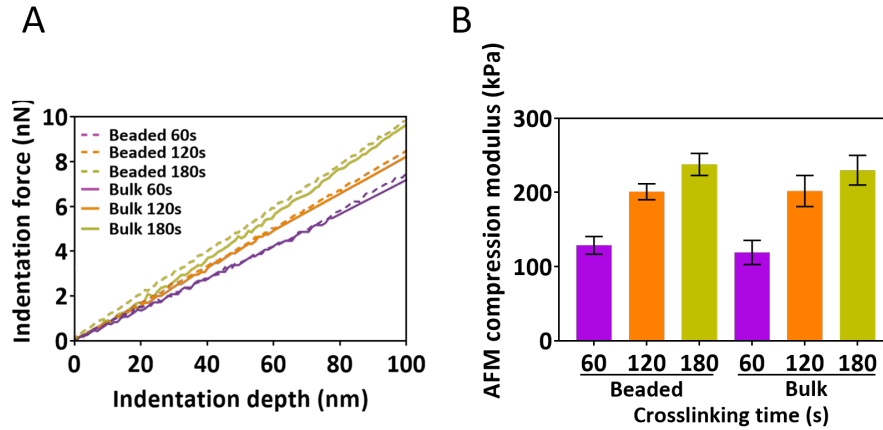


Figure 3.10: (A) Curves displaying the tensile stress vs strain behavior of GelMA microbeads and bulk samples, crosslinked for 60, 120, 180 s. (B) Compressive moduli derived from the stress vs strain curves. It can be appreciated how both GelMA morphologies share comparable stiffness values.

between cells and beads in the scaffold.

3.6.4 Rheology

To conclude the mechanical characterization measurements, rheology is performed to understand the deformability nature of the beaded GelMA scaffold: the storage and loss moduli, G' and G'' , of beaded GelMA scaffolds are measured at increasing angular frequencies through conventional rotational oscillatory rheology techniques. This measurement is essential to understand the behavior of the scaffold in different conditions and therefore derive its possible applications. Depending on the viscous behavior, it may be possible to implement injectable beaded GelMA scaffolds for a myriad of applications such as wound healing, advanced drug delivery and even cavity filling in dentistry. Figure 3.11 shows the rheological behavior of beaded GelMA versus bulk as a function of the angular frequency.

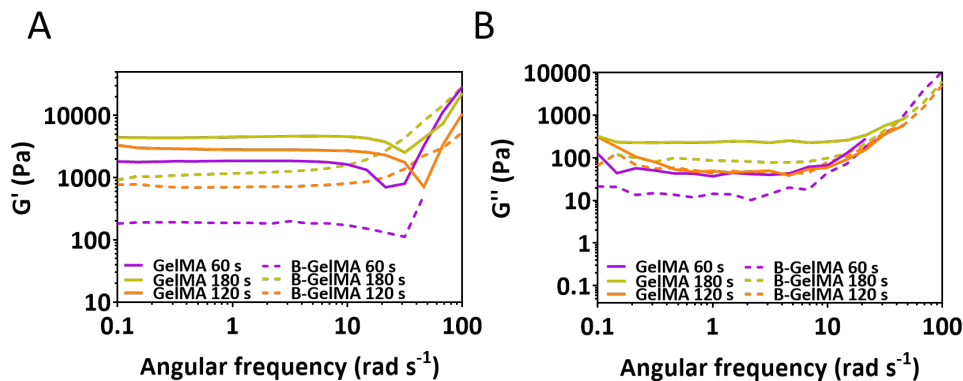


Figure 3.11: Rheological properties of beaded GelMA scaffolds compared to their bulk counterparts in terms of storage (A) and loss (B) moduli versus angular frequency. Range of measurements between 0.1 rad s^{-1} and 100 rad s^{-1}

The plots show the solid-like behavior of both beaded and bulk GelMA scaffolds

at low angular frequencies, in fact the storage moduli are constant at rates below 10 rad s^{-1} . Increasing the frequency, it is possible to notice that the storage and loss moduli both increase, indicating that the scaffold is transitioning towards a glassy behavior [41]. Comparing the curves of beaded and bulk scaffolds, it is possible to notice that the latter generally have a more elastic behavior: this can be explained considering the damping effect present in the beaded scaffolds, due to the larger porosity and most importantly to the friction forces that are present in between the microbeads. The results also confirm that the elasticity of the scaffolds, independently from the type, increases with longer crosslinking time: this can be intuitively deduced from the dynamics of crosslinking, where long polymer chains find themselves bound to each other covalently through the activated photoinitiator, reducing the energy dissipation due to polymer chains sliding against each other.

Figure 3.12 focuses on a particular oscillation rate, set to $\sim 1 \text{ rad s}^{-1}$ circa and compares storage and loss moduli for both types of scaffolds.

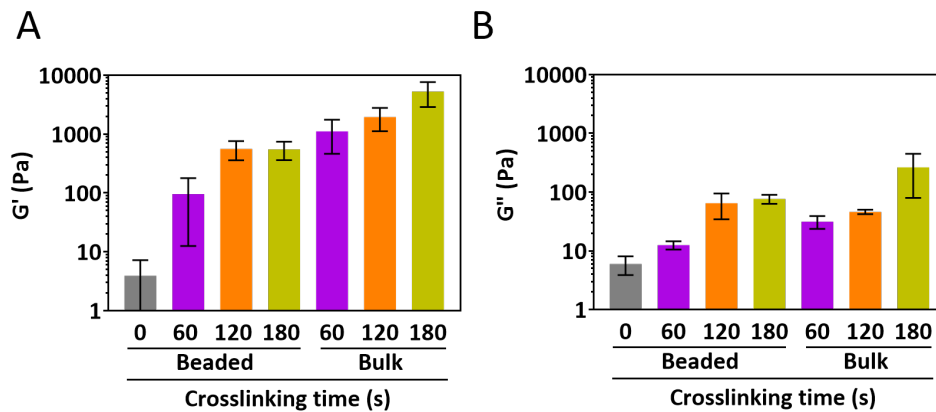


Figure 3.12: (A) Storage moduli at frequency $\sim 1 \text{ rad s}^{-1}$ and $\sim 0.1\%$ strain, evaluated for bulk and beaded GelMA scaffolds. (B) Same as the adjacent image but relative to the loss moduli. 0 crosslinking time in beaded samples indicates non annealed structures.

Finally, it can be concluded that the annealed beaded GelMA scaffolds can be used for Organ-on-a-Chip applications and tissue repair, however the results also mean that these structures are not suitable neither for injection nor other applications that require shape adaptivity, such as fillers. A possible solution for such application can be achieved using partially crosslinked beads that are injected and exposed to UV (or any other crosslinking light) immediately after, directly in situ.

3.7 Cell studies

The final goal of the development of beaded GelMA structures studied in this work is to develop novel scaffolds for 3D cell cultures for a multitude of applications. Therefore it is compulsory to perform studies on cell viability and behavior in such a new environment. In this section there are shown experiments and results proving the compatibility between the scaffold fabrication process and the cell the viability and proliferation. Novel properties are also highlighted, such as high speed cell penetration into the scaffolds, exploiting the characteristics of the porous structure.

All experiments are performed using 20% GelMA, comparing the beaded GelMA scaffolds with the bulk ones, further drawing attention to the novel applications available with the beaded architecture.

3.7.1 Cell encapsulation

The first biology-focused experiments consist in a cell culture study performed by mixing 3T3 cells with a concentrated suspension of physically crosslinked GelMA microbeads to then form solid scaffolds via UV annealing. The methodology followed to perform the cell encapsulation is thoroughly described in section 2.2.13, while the metabolic activity assessment method and live/dead staining protocols are explained in sections 2.2.14 and 2.2.16 respectively.

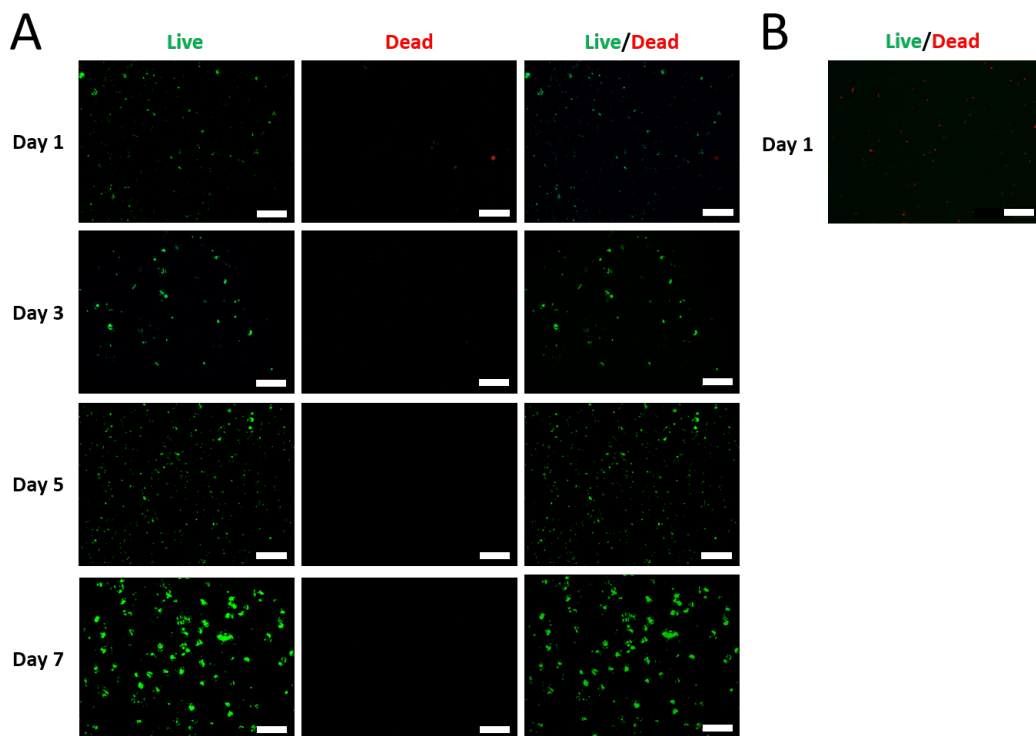


Figure 3.13: (A) Fluorescence microscope images of 3T3 cells embedded inside the beaded GelMA scaffolds after live/dead staining, with timepoints up to day 7 (B) Day 1 live/dead staining of the same cells embedded into bulk GelMA scaffolds. Scale bars indicate 500 μm

Figure 3.13 shows the results of the live/dead staining of the encapsulation experiments. It is interesting to notice how the 3T3 cells keep growing over time, with a negligible amount of cell death. Day 7 images show that cell spreading starts around the first cells that are seeded, occupying as much pore space as possible. Part (B) shows instead that the cells embedded into bulk scaffolds die at day 1: this is the expected result since such a high concentration of GelMA induces very small porosity and high stiffness, compromising the possibility for the cells to spread and therefore inducing their death.

It is possible to quantitatively evaluate the compatibility of the scaffolds with cell cultures: thanks to the viability assay and image processing on the live/dead im-

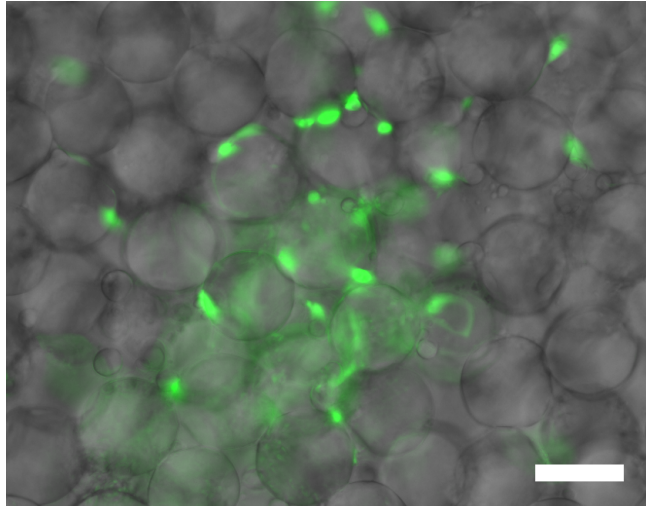


Figure 3.14: Fluorescence and brightfield images overlay, showing a close-up of the beaded GelMA structure, where cell adhering to the beads surface are spreading through the pores. 3T3 cells stained with live/dead staining. Scale bar indicates 100 μm

ages it is possible to measure the amount of viable cells and their activity. The PrestoBlueTM does not induce cell death, meaning that the same scaffold are monitored at every timepoint, moreover it can be implemented in multiple-well plates and analyzed using a well plate reader, making high throughput quantification possible. Another advantage of the assay is that it permeates the whole sample, overcoming the limitation caused by the field of view when imaging the live/dead stained cells. Figure 3.15 shows the results of such measurements.

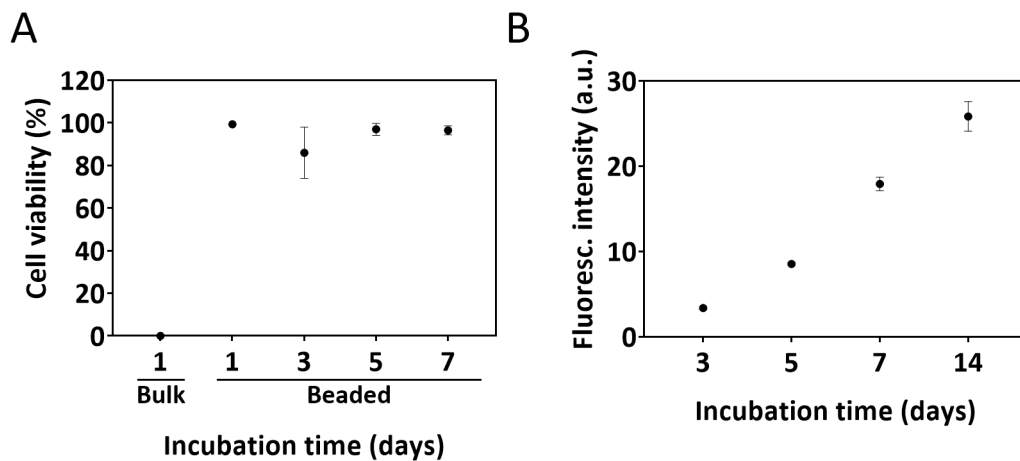


Figure 3.15: (A) Plot indicating the ratio between live and dead cells in the images displayed in figure 3.13 (B) PrestoBlueTM assay fluorescence intensity readings, performed up to 14 days after incubation.

As expected, the viable cells in the beaded GelMA constitute the majority, while the bulk GelMA scaffolds are a harsh environment for cell growth inducing death at day 1.

3.7.2 Cell penetration

Given the porous geometry of the beaded GelMA scaffolds, it is expected that cells will tend to migrate and penetrate through the structure. This is a feature that is hardly achievable in the bulk counterparts, where the entangled polymer chains network induces sub micron-sized pores, reducing the spatial freedom for the cells. The goal of this experiment is to validate such hypothesis by pipetting a cell suspension of HUVEC cells over beaded and bulk GelMA scaffold, following the procedure described in section 2.2.15.

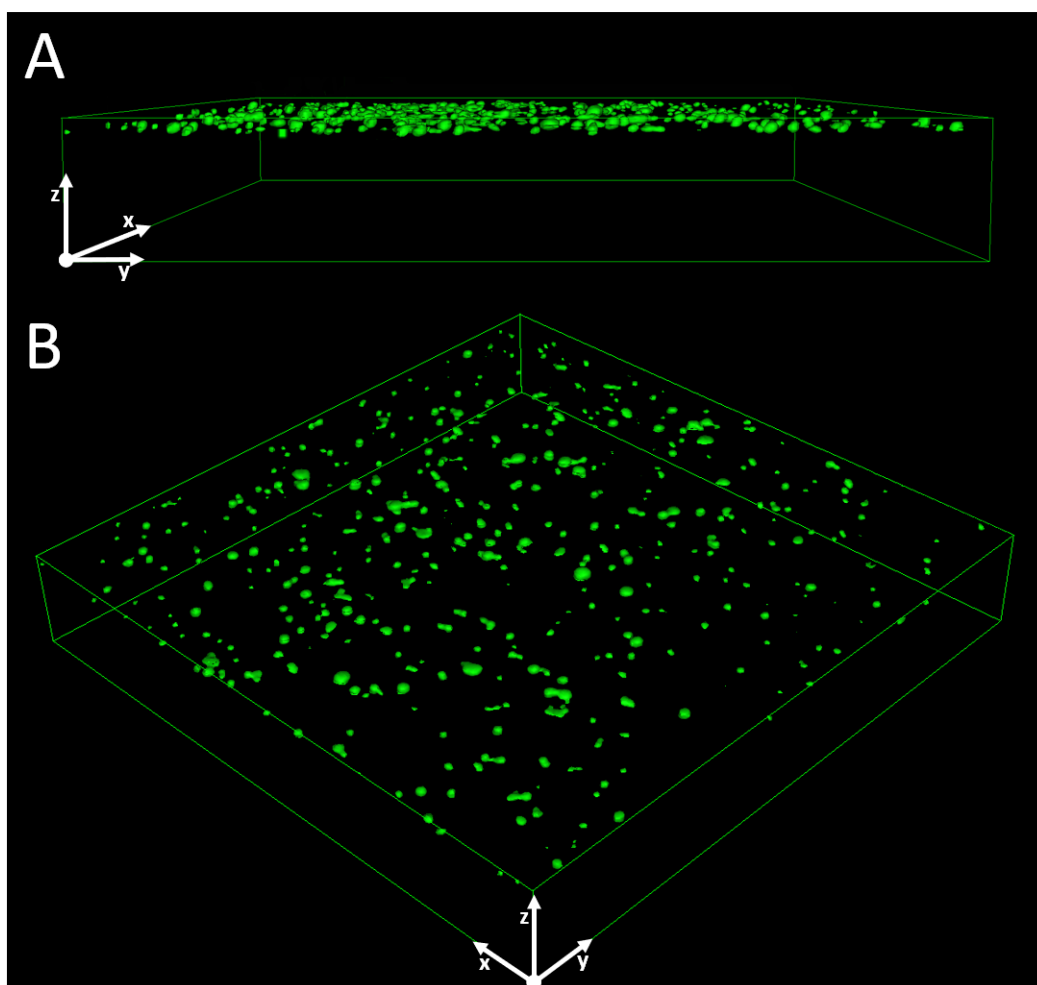


Figure 3.16: (A) Lateral view of the 3D reconstruction representing the cell penetration of the HUVEC cells into a bulk GelMA substrate, after 1 hour (B) Orthographic view of the same. Sides are $1550\ \mu\text{m}$ long and height is $254\ \mu\text{m}$ high

Figure 3.16 shows the first experiment performed on a bulk substrate, showing the still circular cells laying on the top surface of the sample, an expected behavior. Some of the cells are already adhering, spreading flatter on the surface: over time the majority would stick to the 20% GelMA and proliferate as if cultured on top of a regular plastic substrate used in routine cell cultures.

Figure 3.17 shows the analogous beaded sample: it is straightforward to notice that the cells have quickly penetrated through the entire scaffold, some reaching the bottom surface in contact with the supporting microscope slide. Given the methodology followed, dispensing the cell suspension from the top, it can be deduced that

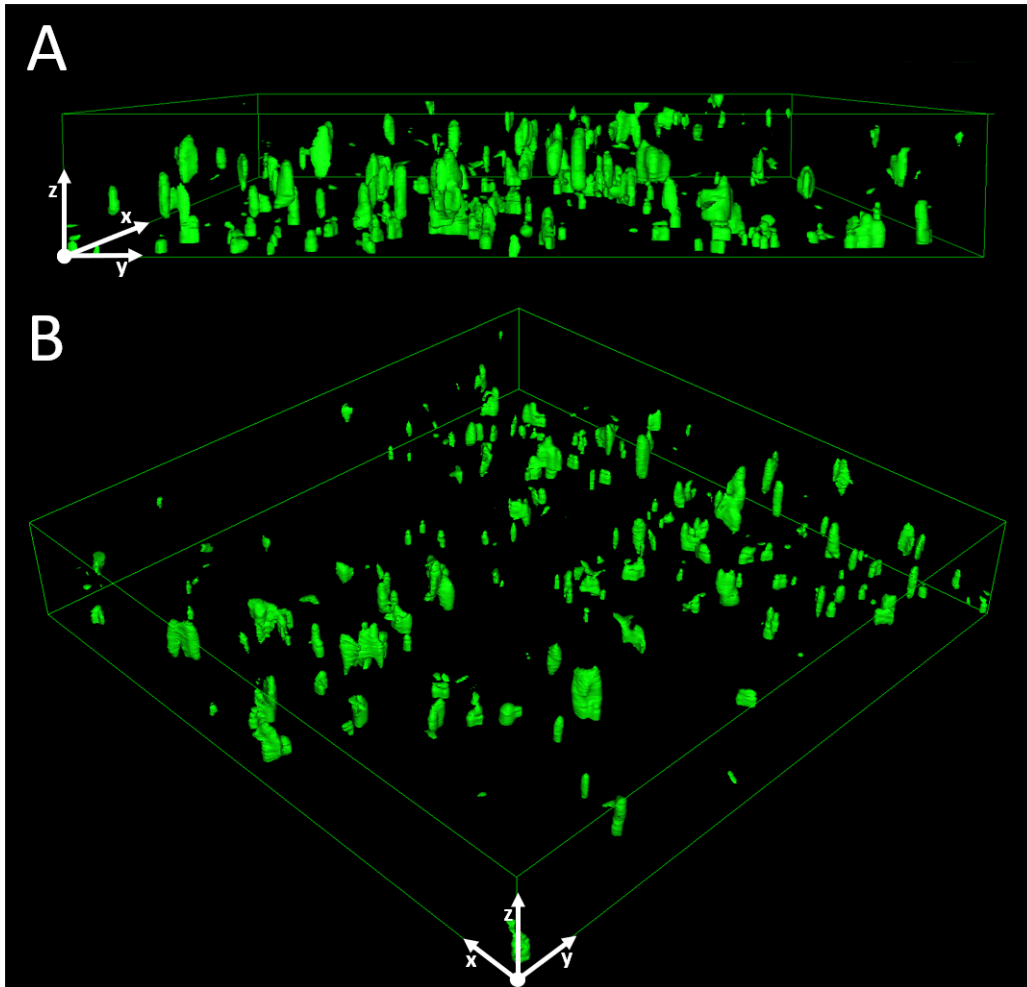


Figure 3.17: (A) Lateral view of the 3D reconstruction representing the cell penetration of the HUVEC cells into a beaded GelMA substrate, after 1 hour (B) Orthographic view of the same. Sides are $1550\ \mu\text{m}$ long and height is $254\ \mu\text{m}$ high

this migration phenomenon is driven by both capillarity and gravity: the first is faster since water (or cell media) naturally infiltrates the pores, further hydrating the entire scaffold. Gravity is then driving the cells towards the bottom, because of their low buoyancy in media, making them sink. The sample thickness in both experiments is set to $\sim 0.3\ \text{mm}$, a relatively low value chosen in order to successfully image the cells throughout the whole scaffold and avoid diffraction effects due to the multiple microbeads layers that are before the confocal microscope objective. Imagining a thicker sample, cells would hardly reach the bottom, gradually settling down on the microbeads surfaces. As a final note to the reader, the shape of the features shown in this figure can be explained considering the fact that cells might have formed aggregates while penetrating the scaffolds, moreover some cells might be also still moving through if not attached yet to the beads.

Finally, since the penetration experiments confirmed the previously formulated hypotheses, it can be deduced that cell migration can be achieved providing an appropriate driving force: capillarity, gravity, flow and the application of chemokines can pull or push cells through the tunable pores, making it possible to perform a new class of experiments not available when using bulk hydrogel scaffolds.

Chapter 4

Conclusions and Perspectives

4.1 Conclusions

In this work, a novel application of GelMA microbeads, generated with the help of droplet microfluidics has been introduced: a robust and simple bead manipulation protocol has been developed, allowing the extraction of the GelMA microspheres from the oil suspension, exploiting the temperature-based physical crosslinking of the polymer. Doing so, a reduced number of chemical treatments are needed, making the process more favorable for the culturing of sensitive cell lines. Moreover, such approach allows the creation of scaffold constituted by GelMA microbeads enriched mixing other chemicals, such as mineral crystals or drugs, expanding the possible applications of the platform.

Following, a thorough characterization work is performed on the beads, both individually and when annealed in a self-standing structure: first the construction of self standing scaffolds is validated, macroscopically and at the micron scale. Then a temperature dependence study is performed to understand the behavior of crosslinked and non-crosslinked individual beads under different environments, showing that crosslinked samples can withstand cell incubation temperatures. Also, the swelling and shrinking of single microbeads is measured immersing them in two different ionic strength solutions, namely deionized water and high salinity PBS, and therefore confirming the stability conferred by the chemical crosslinking. The scaffold porosity is evaluated with the help of confocal microscopy, showing a large pore size suitable for cell infiltration and proliferation. Following, a set of mechanical characterization measurements have been performed: compression studies on beaded scaffolds showed that it is possible to obtain similar stiffnesses as their bulk counterparts, tensile studies showed the low force values holding the beads together, rheology studies confirmed the similar viscoelastic properties as bulk scaffolds. Finally compression measurements performed on single beads, with the help of an Atomic Force Microscopy setup, validated that the microbead handling protocol has not altered the GelMA mechanical properties, since both beads and bulk samples have shown similar values.

Finally, cell culturing studies have been successfully performed using two different techniques, validating the possibility to use the newly developed GelMA beaded scaffolds for tissue engineering. Mixing cells and bead suspensions together and annealing the mixture, it has been experimentally proven that the microbead handling protocol is cell-friendly and compatible with any encapsulation experiment.

Secondly, cell penetration experiments have show that the porosity of the scaffolds facilitates both percolation and migration, opening new possibilities of experiments on cell migration, such as in cell intravasation and extravasation proper of metastasis in vitro models.

4.2 Perspectives

This work validated the promising properties of GelMA-based 3D scaffolds for the various application possible in tissue engineering. In this last section, a set of proposed projects and experiments are briefly described, leaving the work to the future hard-working and creative scientists interested in this platform.

A first expansion might the encapsulation of cells inside individual beads: to achieve uniform distributions in each droplet, new microfluidics should be designed and tested. Then the handling protocol should be tested and, if effective, a new set of applications would become possible. This way spheroids of uniform size could be produced, in the same fashion as in other works carried using other biomaterials

Another intriguing experiment would exploit the high porosity of the beaded scaffolds to create highly vascularized tissues in vitro, using endothelial cells: the biological experiments performed in this work confirm the possibility of tightly embedding cells in between beads. A further evolution can be the implementation of a continuous media flow through the scaffold, simulating blood flow and interacting with the cells adhering to the beads, using a specifically designed and simple microfluidic device to confine the flow inside the structure. Leveraging on the results that could be obtained in these two proposed experiments, an important step forward could be achieved in the fabrication of large scale functional Organs-on-a-Chip: cell encapsulated in properly-sized beads would then form spheroids, but thanks to the vascularization, these would not overgrow and therefore would have negligible, if not even absent, necrotic cores.

Bibliography

- [1] Sam H. Au et al. “Hepatic organoids for microfluidic drug screening”. In: *Lab on a Chip* 14.17 (2014), pp. 3290–3299. ISSN: 14730189.
- [2] Jean Berthier. “Chapter 3 - The Physics of Droplets**This chapter was written with the collaboration of Kenneth A. Brakke (Mathematics Department, Susquehanna University, Selinsgrove, PA).” In: *Micro and Nano Technologies*. Ed. by Jean B T - Micro-Drops Berthier and Digital Microfluidics (Second Edition). William Andrew Publishing, 2013, pp. 75–160. ISBN: 978-1-4557-2550-2.
- [3] Sílvia J. Bidarra, Cristina C. Barrias, and Pedro L. Granja. “Injectable alginate hydrogels for cell delivery in tissue engineering”. In: *Acta Biomaterialia* 10.4 (2014), pp. 1646–1662. ISSN: 18787568.
- [4] David J Collins et al. “The Poisson distribution and beyond: methods for microfluidic droplet production and single cell encapsulation”. In: *Lab on a Chip* 15.17 (2015), pp. 3439–3459. ISSN: 1473-0197.
- [5] “Current Applications of Tissue Engineering in Biomedicine”. In: *Journal of Biochips & Tissue Chips* s2 (Aug. 2015), pp. 1–14. ISSN: 21530777.
- [6] Jeanie L. Drury and David J. Mooney. “Hydrogels for tissue engineering: Scaffold design variables and applications”. In: *Biomaterials* 24.24 (2003), pp. 4337–4351. ISSN: 01429612. arXiv: arXiv:1011.1669v3.
- [7] David C. Duffy et al. “Rapid prototyping of microfluidic systems in poly(dimethylsiloxane)”. In: *Analytical Chemistry* 70.23 (1998), pp. 4974–4984. ISSN: 00032700. arXiv: 1106.3015.
- [8] Kimberly M. Ferlin et al. “Influence of 3D printed porous architecture on mesenchymal stem cell enrichment and differentiation”. In: *Acta Biomaterialia* 32 (2016), pp. 161–169. ISSN: 18787568.
- [9] Allan J Franko and Robert M Sutherland. “Oxygen Diffusion Distance and Development of Necrosis in Multicell Spheroids”. In: *Radiation Research* 79.3 (1979), pp. 439–453. ISSN: 00337587, 19385404.
- [10] *GLOBOCAN 2012: Estimated Cancer Incidence Mortality and Prevalence Worldwide in 2012*. 2012.
- [11] GODT. “Organ Donation and Transplantation Activities 2015 Report”. In: *Organ Donation and Transplantation Activities, 2015 Report ; 2017* September (2016), pp. 1–51.
- [12] Donald R. Griffin et al. “Accelerated wound healing by injectable microporous gel scaffolds assembled from annealed building blocks”. In: *Nature Materials* 14.7 (2015), pp. 737–744. ISSN: 14764660.

- [13] Pierre Guillot, Annie Colin, and Armand Ajdari. “Stability of a jet in confined pressure-driven biphasic flows at low Reynolds number in various geometries”. In: *Physical Review E* 78.1 (July 2008), p. 16307.
- [14] Thomas C. Hales. “Historical overview of the Kepler conjecture”. In: *Discrete and Computational Geometry* 36.1 (2006), pp. 5–20. ISSN: 14320444. arXiv: 9811071 [math].
- [15] Kentaro Hayashi and Yasuhiko Tabata. “Preparation of stem cell aggregates with gelatin microspheres to enhance biological functions”. In: *Acta Biomaterialia* 7.7 (2011), pp. 2797–2803. ISSN: 1742-7061.
- [16] K. L. Johnson. *Contact Mechanics*. Cambridge: Cambridge University Press, 1985. ISBN: 9781139171731.
- [17] Juan Liu et al. “Hydrogels for engineering of perfusable vascular networks”. In: *International Journal of Molecular Sciences* 16.7 (2015), pp. 15997–16016. ISSN: 14220067. arXiv: 15334406.
- [18] Yukiko T. Matsunaga, Yuya Morimoto, and Shoji Takeuchi. “Molding cell beads for rapid construction of macroscopic 3D tissue architecture”. In: *Advanced Materials* 23.12 (2011), pp. 90–94. ISSN: 09359648.
- [19] W F Neuman and M W Neuman. “The Nature of the Mineral Phase of Bone.” In: *Chemical Reviews* 53.1 (Aug. 1953), pp. 1–45. ISSN: 0009-2665.
- [20] Anamika R. Pandey et al. “Chitosan: Application in tissue engineering and skin grafting”. In: *Journal of Polymer Research* 24.8 (2017). ISSN: 15728935.
- [21] Francesco Piraino et al. “Multi-gradient hydrogels produced layer by layer with capillary flow and crosslinking in open microchannels”. In: *Lab on a Chip* 12.3 (Feb. 2012), pp. 659–661. ISSN: 1473-0197.
- [22] “PrestoBlue Cell Viability Reagent for Microplates Protocol - US”. In: ().
- [23] Qasem Ramadan and Martin A.M. Gijs. “In vitro micro-physiological models for translational immunology”. In: *Lab on a Chip* 15.3 (2015), pp. 614–636. ISSN: 14730189.
- [24] Jelena Rnjak-Kovacina and Anthony S. Weiss. “Increasing the Pore Size of Electrospun Scaffolds”. In: *Tissue Engineering Part B: Reviews* 17.5 (2011), pp. 365–372. ISSN: 1937-3368.
- [25] S B Ross-Murphy and H McEvoy. “Fundamentals of hydrogels and gelation”. In: *British Polymer Journal* 18.1 (1986), pp. 2–7.
- [26] Johannes Schindelin et al. “Fiji: An open-source platform for biological-image analysis”. In: *Nature Methods* 9.7 (2012), pp. 676–682. ISSN: 15487091. arXiv: 1081-8693.
- [27] Elias Sideris et al. “Particle Hydrogels Based on Hyaluronic Acid Building Blocks”. In: *ACS Biomaterials Science and Engineering* 2.11 (2016), pp. 2034–2041. ISSN: 23739878.
- [28] Aleksander Skardal et al. “Multi-tissue interactions in an integrated three-tissue organ-on-a-chip platform”. In: *Scientific Reports* 7.1 (2017), pp. 1–16. ISSN: 20452322.

- [29] Fernandez Stephanie et al. “Towards the fabrication of a 3D printed vascularized islet transplantation device for the treatment of type 1 diabetes”. In: *Frontiers in Bioengineering and Biotechnology* 4 (2016). ISSN: 2296-4185.
- [30] Mark W. Tibbitt and Kristi S. Anseth. “Hydrogels as extracellular matrix mimics for 3D cell culture”. In: *Biotechnology and Bioengineering* 103.4 (2009), pp. 655–663. ISSN: 00063592. arXiv: NIHMS150003.
- [31] Raja K. Vadivelu et al. “Microfluidic technology for the generation of cell spheroids and their applications”. In: *Micromachines* 8.4 (2017), pp. 1–23. ISSN: 2072666X.
- [32] An I. Van Den Bulcke et al. “Structural and rheological properties of methacrylamide modified gelatin hydrogels”. In: *Biomacromolecules* 1.1 (2000), pp. 31–38. ISSN: 15257797.
- [33] Christopher G. Williams et al. “Variable cytocompatibility of six cell lines with photoinitiators used for polymerizing hydrogels and cell encapsulation”. In: *Biomaterials* 26.11 (2005), pp. 1211–1218. ISSN: 01429612.
- [34] Denis Wirtz, Konstantinos Konstantopoulos, and Peter C Searson. “The physics of cancer: the role of physical interactions and mechanical forces in metastasis”. In: *Nature Reviews Cancer* 11 (June 2011), p. 512.
- [35] Xin Xiao et al. “The promotion of angiogenesis induced by three-dimensional porous beta-tricalcium phosphate scaffold with different interconnection sizes via activation of PI3K/Akt pathways”. In: *Scientific Reports* 5 (2015), pp. 1–11. ISSN: 20452322.
- [36] Kan Yue et al. “Synthesis, properties, and biomedical applications of gelatin methacryloyl (GelMA) hydrogels”. In: *Biomaterials* 73 (2015), pp. 254–271. ISSN: 18785905. arXiv: NIHMS150003.
- [37] Michele Zanoni et al. “3D tumor spheroid models for in vitro therapeutic screening: A systematic approach to enhance the biological relevance of data obtained”. In: *Scientific Reports* 6. August 2015 (2016), pp. 1–11. ISSN: 20452322.
- [38] Yu Shrike Zhang, Yi Nan Zhang, and Weijia Zhang. “Cancer-on-a-chip systems at the frontier of nanomedicine”. In: *Drug Discovery Today* 22.9 (2017), pp. 1392–1399. ISSN: 18785832. arXiv: NIHMS150003.
- [39] Yu Shrike Zhang et al. “Multisensor-integrated organs-on-chips platform for automated and continual in situ monitoring of organoid behaviors”. In: *Proceedings of the National Academy of Sciences* 114.12 (2017), E2293–E2302. ISSN: 0027-8424. arXiv: arXiv:1408.1149.
- [40] Xin Zhao et al. “Cell infiltrative hydrogel fibrous scaffolds for accelerated wound healing”. In: *Acta Biomaterialia* 49 (2017), pp. 66–77. ISSN: 1742-7061.
- [41] Jonathan M. Zuidema et al. “A protocol for rheological characterization of hydrogels for tissue engineering strategies”. In: *Journal of Biomedical Materials Research - Part B Applied Biomaterials* 102.5 (2014), pp. 1063–1073. ISSN: 15524981.